Atmospheric
Chemistry
and Physics

The formation and mitigation of nitrate pollution: comparison between urban and suburban environments

Suxia Yang[1,2], Bin Yuan[1,2], Yuwen Peng[1,2], Shan Huang[1,2], Wei Chen[3], Weiwei Hu[3], Chenglei Pei[3,4,5,6],
Jun Zhou[1,2], David D. Parrish[1], Wenjie Wang[7], Xianjun He[1,2], Chunlei Cheng[2,8], Xiao-Bing Li[1,2],
Xiaoyun Yang[1,2], Yu Song[7], Haichao Wang[9], Jipeng Qi[1,2], Baolin Wang[10], Chen Wang[10],
Chaomin Wang[1,2], Zelong Wang[1,2], Tiange Li[1,2], E Zheng[1,2], Sihang Wang[1,2], Caihong Wu[1,2],
Mingfu Cai[1,2], Chenshuo Ye[7], Wei Song[3], Peng Cheng[8], Duohong Chen[6], Xinming Wang[3],
Zhanyi Zhang[1,2], Xuemei Wang[1,2], Junyu Zheng[1,2], and Min Shao[1,2]

[1]Institute for Environmental and Climate Research, Jinan University, Guangzhou 511443, China
[2]Guangdong-Hongkong-Macau Joint Laboratory of Collaborative Innovation for Environmental Quality,
Jinan University, Guangzhou 511443, China
[3]State Key Laboratory of Organic Geochemistry, Guangzhou Institute of Geochemistry, Chinese Academy of
Sciences, Guangzhou 510640, China
[4]CAS Center for Excellence in Deep Earth Science, Guangzhou, 510640, China
[5]University of Chinese Academy of Sciences, Beijing 100049, China
[6]Guangzhou Ecological and Environmental Monitoring Center of Guangdong Province,
Guangzhou 510060, China
[7]State Joint Key Laboratory of Environmental Simulation and Pollution Control, College of Environmental
Sciences and Engineering, Peking University, Beijing 100871, China
[8]Institute of Mass Spectrometry and Atmospheric Environment, Guangdong Provincial Engineering Research
Center for on-line Source Apportionment System of Air Pollution, Jinan University, Guangzhou 510632, China
[9]School of Atmospheric Sciences, Sun Yat-Sen University, Guangzhou 510275, China
[10]School of Environmental Science and Engineering, Qilu University of Technology, Jinan 250353, China

Correspondence: Bin Yuan (byuan@jnu.edu.cn) and Min Shao (mshao@pku.edu.cn)

Abstract. Ambient nitrate has been of increasing concern in $PM_{2.5}$, while there are still large uncertainties in quantifying the formation of nitrate aerosol. The formation pathways of nitrate aerosol at an urban site and a suburban site in the Pearl River Delta (PRD) are investigated using an observation-constrained box model. Throughout the campaigns, aerosol pollution episodes were constantly accompanied with the increase in nitrate concentrations and fractions at both urban and suburban sites. The simulations demonstrate that chemical reactions in the daytime and at night both contributed significantly to formation of nitrate in the boundary layer at the two sites. However, nighttime reactions predominantly occurred aloft in the residual layer at the urban site, and downward transport from the residual layer in the morning is an important source (53 %) for surface nitrate at the urban site, whereas similar amounts of nitrate were produced in the nocturnal boundary layer and residual layer at the suburban site, which results in little downward transport of nitrate from the residual layer to the ground at the suburban site. We show that nitrate formation was in the volatile-organic-compound-limited (VOC-limited) regime at the urban site, and in the transition regime at the suburban site, identical to the response of ozone at both sites. The reduction of VOC emissions can be an efficient approach to mitigate nitrate in both urban and suburban areas through influencing hydroxyl radical (OH) and N_2O_5 production, which will also be beneficial for the synergistic control of regional ozone pollution. The results highlight that the relative importance of nitrate formation pathways and ozone can be site-specific, and the quantitative understanding of various pathways of nitrate formation will provide insights for developing nitrate and ozone mitigation strategies.

1 Introduction

Particulate nitrate is a substantial chemical component of fine particles, which plays a significant role in the acid deposition, visibility reduction, hygroscopic properties, and radiative forcing (Li et al., 1993; Watson, 2002; Pathak et al., 2009; Xu and Penner, 2012; Zhang et al., 2017; Liu et al., 2020). Due to the larger emission reduction of SO_2 than NO_x and little change in NH_3 since the implementation of the clean air actions in China (Guo et al., 2018; M. Liu et al., 2019; Zhai et al., 2021), a considerable increase in the nitrate fractions in aerosols has been observed in haze periods in the northern China Plain (Wen et al., 2018; Li et al., 2018; Lu et al., 2013; Fu et al., 2020), southern China (Pathak et al., 2009, 2011), and eastern China (Griffith et al., 2015; Tao et al., 2018; Yun et al., 2018b; Li et al., 2018), which indicates the growing significance of nitrate in the formation of haze events. In addition, the photolysis of particulate nitrate can increase the production of sulfate and nitrous acid (HONO), implying the importance of nitrate in the synergetic enhancement of the atmospheric oxidizing capability in haze events (Gen et al., 2019; Zhang et al., 2020; Ye et al., 2016, 2017), although the photolysis of particulate nitrate to produce HONO still remains highly uncertain (Romer et al., 2018). Hence, identifying and understanding the driving factors of nitrate formation are essential to establishment of optimized mitigation policies for fine particles.
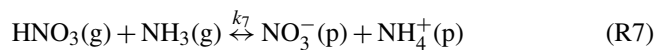
Particulate inorganic nitrate is primarily produced through two processes: the photochemical reaction of hydroxyl radical (OH) and NO_2 during daytime (Reaction R1) and the heterogeneous uptake of N_2O_5 (Reactions R2–R5) during nighttime. The gaseous nitric acid (HNO_3) is produced by the reaction of OH and NO_2 and then reacts with ammonia (NH_3) to form particulate nitrate (Stelson and Seinfeld, 1982). The partitioning process of HNO_3 between the gas and particle phase is regulated by ambient temperature (T), relative humidity (RH) (Mozurkewich, 1993), aerosol pH, and the abundance of NH_3 (Reaction R7) (Xue et al., 2014a; Yun et al., 2018b; Franchin et al., 2018). The pH value within a certain range plays an important role in the gas-particle partitioning of nitrate, which significantly impacts the nitrate formation (Guo et al., 2018; Lawal et al., 2018; Nenes et al., 2020).

$$OH + NO_2 \xrightarrow{k_1} HNO_3(g) \tag{R1}$$

$$NO_2 + O_3 \xrightarrow{k_3} NO_3 + O_2 \tag{R2}$$

$$NO_3 + NO_2 \overset{k_4}{\leftrightarrow} N_2O_5 \tag{R3}$$

$$NO_3 + VOCs \rightarrow products \tag{R4}$$

$$N_2O_5 + \left(H_2O \text{ or } Cl^-\right) \xrightarrow{k_5} \varphi ClNO_2 + (2 - \varphi) NO_3^-(p) \tag{R5}$$

$$k_5 = \frac{\omega 1 \cdot \gamma \cdot S_a}{4} \tag{1}$$

$$ClNO_2 \xrightarrow{k_6} Cl \cdot + NO_2 \tag{R6}$$

$$k_6 = J_{ClNO_2} \tag{2}$$

$$HNO_3(g) + NH_3(g) \overset{k_7}{\leftrightarrow} NO_3^-(p) + NH_4^+(p) \tag{R7}$$

The heterogeneous uptake reaction of N_2O_5 can occur on the surface of water or chlorine-containing particles (Reaction R5), and the reaction constant (k_5) is described by Eq. (1), where φ is the production yield of $ClNO_2$ in Reaction (R5), ω_1 is the average molecular speed of N_2O_5 ($m\,s^{-1}$), γ is the uptake coefficient of N_2O_5, and S_a ($m^2\,m^{-3}$) is the aerosol surface area concentration in Eq. (1). The nitryl chloride ($ClNO_2$) produced by the heterogeneous uptake reaction of N_2O_5 at night would photolyze the next morning, which would produce chlorine atoms and NO_2 (Reaction R6). Here the reaction rate k_6 was denoted as the photolysis rate of $ClNO_2$ (J_{ClNO_2}). The heterogeneous uptake reaction of N_2O_5 is affected by the uptake coefficient (γ) and the production yield of $ClNO_2$ (φ), which cannot be directly measured and are significantly impacted by the aerosol components and ambient RH (Bertram and Thornton, 2009; Bian et al., 2017; McDuffie et al., 2018a, b). Thus, the nocturnal contribution to nitrate formation still has great uncertainty.

With the radiative cooling in the afternoon, the mixed layer decoupled into a steady, near-surface nocturnal boundary layer (NBL) and a residual layer (RL), which is a neutral layer and formed aloft during the turbulence attenuation process (Prabhakar et al., 2017). The heterogeneous uptake of N_2O_5 in the nocturnal boundary layer is greatly disturbed in the presence of fresh NO emissions, which titrate the NO_3 radical within the stagnant boundary layer (Geyer and Stutz, 2004; Li et al., 2020; Chen et al., 2020). However, aircraft observations in California and Utah in the US have revealed that active uptake of N_2O_5 in the residual layer contributed a major portion of the near-surface nitrate accumulation during the morning transport from aloft (Brown et al., 2006; Chow et al., 2006; Prabhakar et al., 2017; McDuffie et al., 2019; Womack et al., 2019). Similarly, ground- and tower-based field observations also pointed out the important contribution of this pathway to the rapid increase in near-surface nitrate concentrations in Beijing, China (Wang et al., 2018a; Chen et al., 2020). However, under different atmospheric conditions, the relative importance of nitrate production varies significantly within the residual layer (McDuffie et al., 2019; Tang et al., 2021), giving widely varying relative contributions of the major chemical pathways to nitrate pollution among different sites (Wang et al., 2018a; Womack et al., 2019; Chen et al., 2020; Lin et al., 2020). A comprehensive understanding of the nitrate production in the residual layer is required to quantify the contributions of different formation pathways to nitrate pollution.

The nitrate production from the reaction of OH and NO_2 pathway during daytime is well-understood, and the control of NO_x emission is commonly considered as an effective strategy to reduce ambient nitrate. However, several studies

reported that the efficiency of NO_x reduction in nitrate control is limited, and it may enhance nitrate production under some conditions (Womack et al., 2019; Dong et al., 2014; Hou et al., 2019). The study by Womack et al. (2019) showed that both nitrate and ozone were VOC-limited in Salt Lake City, suggesting that VOC control would effectively reduce nitrate. Similarly, modeling studies also found that the nitrate formation was more sensitive to the change in VOC concentrations over the northern and eastern China (Dong et al., 2014; Lu et al., 2019; Fu et al., 2020). The sensitivity of nitrate production to both NO_x and VOCs in different regions should be comparatively evaluated, which could provide helpful implications in formulating effective control strategies for the mitigation of aerosol pollution.

In recent years, the nitrate formation in haze episodes has been studied in northern China (Liu et al., 2015; Wang et al., 2017a; Wen et al., 2018; Fu et al., 2020; Chen et al., 2020), eastern China (Tao et al., 2016; Lin et al., 2020), and southern China (Qin et al., 2017; Tao et al., 2018; Yun et al., 2018b; Su et al., 2020), and the important contribution of the heterogeneous uptake of N_2O_5 at nighttime has been discussed (Wang et al., 2017b; Yun et al., 2018a, b; Chen et al., 2020). However, these ground-based observations rarely considered the potential contributions of reactive uptake of N_2O_5 aloft in the residual layer, which could be an important source of near-surface nitrate concentrations. In addition, few studies have comprehensively evaluated the relative influence of NO_x and VOC reductions on nitrate production in the urban and suburban areas (Hou et al., 2019).

In this study, we present the results from the ground- and tower-based measurements in both urban and suburban areas in southern China. An observation-constrained box model was used to simulate the production rates of nitrate from different formation pathways, and to compare the effects of reducing NO_x and VOC emissions in both urban and suburban areas. This work provides new insights into the synergetic mitigation of particle and ozone pollution, which can guide development of the most effective nitrate control strategies.

2 Method and data

2.1 Field observation

The ground-based field measurements were conducted at both an urban site in Guangzhou and a suburban site in Heshan. The tower-based measurements were conducted at an urban site in Guangzhou. The ground-based study in Guangzhou was carried out from late September to mid-November 2018 at the Guangzhou Institute of Geochemistry (GIG), Chinese Academy of Sciences (23.1° N, 113.2° E), which is a typical urban site surrounded by a residential area and traffic avenues (Fig. 1). The instruments were deployed on the top of the 25 m building at the GIG site. The ground-based measurement at the suburban site was performed from late September to mid-November 2019 at the

supersite of Heshan county (22.7° N, 112.9° E), which is approximately 50 km southwest of Foshan and 80 km southwest of Guangzhou and is frequently influenced by anthropogenic emissions from upwind Guangzho–Foshan megacity areas. The tower-based measurements were conducted simultaneously at the ground and 448 m on the Canton Tower from late September to mid-November 2018 concurrent with the measurements at the GIG site, which is approximately 5.7 km away (Fig. 1).

The chemical components of PM_1, trace gases, and non-methane hydrocarbons (NMHC) as well as particle BC content and particle size distribution were both measured at the GIG and Heshan sites, whereas only trace gases (NO_x and O_3) and meteorological parameters were measured at the Canton Tower site. The non-refractory chemical compositions of PM_1 (NR-PM_1), including organics (Org), sulfate (SO_4^{2-}), nitrate (NO_3^-), ammonium (NH_4^+), and chloride (Cl^-), were measured using a high-resolution time-of-flight aerosol mass spectrometer (HR-ToF-AMS, Aerodyne Research Inc., US) (Hu et al., 2016; Chen et al., 2021). Black carbon (BC) was measured using an Aethalometer (AE33, Magee Scientific Co., US). Particle number size distribution was measured using a scanning mobility particle sizer with an aerodynamic diameter ranging from 10 to 650 nm (SMPS, TSI, US) and aerosol particle sizer ranging from 500 nm to 20 μm (APS, TSI, US). Details on the limit of detection and accuracy of the instruments are presented in Tables S1–S3.

HNO_3, N_2O_5, and $ClNO_2$ were measured using iodide time-of-flight chemical ionization mass spectrometry (Iodide-TOF-CIMS, Aerodyne Research Inc., US) (Wang et al., 2020b; Ye et al., 2021). The non-methane hydrocarbons (NMHC) were measured using online GC-MS-FID (Wuhan Tianhong Co., Ltd, China) (Yuan et al., 2012) (Table S4). The concentrations of oxygenated VOCs (OVOCs, including formaldehyde (HCHO) and acetaldehyde (CH_3CHO)), the sum of methyl vinyl ketone (MVK), and methacrolein (MACR) were measured via high-resolution proton transfer reaction time-of-flight mass spectrometry (PTR-ToF-MS, Ionicon Analytik, Austria) (Wang et al., 2020a; Wu et al., 2020). HONO was detected using a long-path absorption photometer (LOPAP) at the GIG site (Yu et al., 2021) and was measured by the gas and aerosol collector (GAC) instrument at the Heshan site (Dong et al., 2012; Yang et al., 2014). NH_3 was also measured by two sets of instruments: cavity ring-down spectroscopy (CRDS, Picarro, US) was used at the GIG site, and the GAC instrument was used at the Heshan site (von Bobrutzki et al., 2010).

In addition, trace gases (O_3 (49i), NO_x (42i), CO (48i), and SO_2 (43i)) (Thermo Scientific, US) and meteorological parameters (i.e., wind speed (WS), wind direction (WD), temperature (T), relative humidity (RH), and pressure (P)) (Vantage Pro 2, Davis Instruments Co., US) were simultaneously measured during these campaigns. The photolysis frequencies of O_3, NO_2, HCHO, and HONO (PFS-100, Focused Photonics Inc., China) were also measured during the
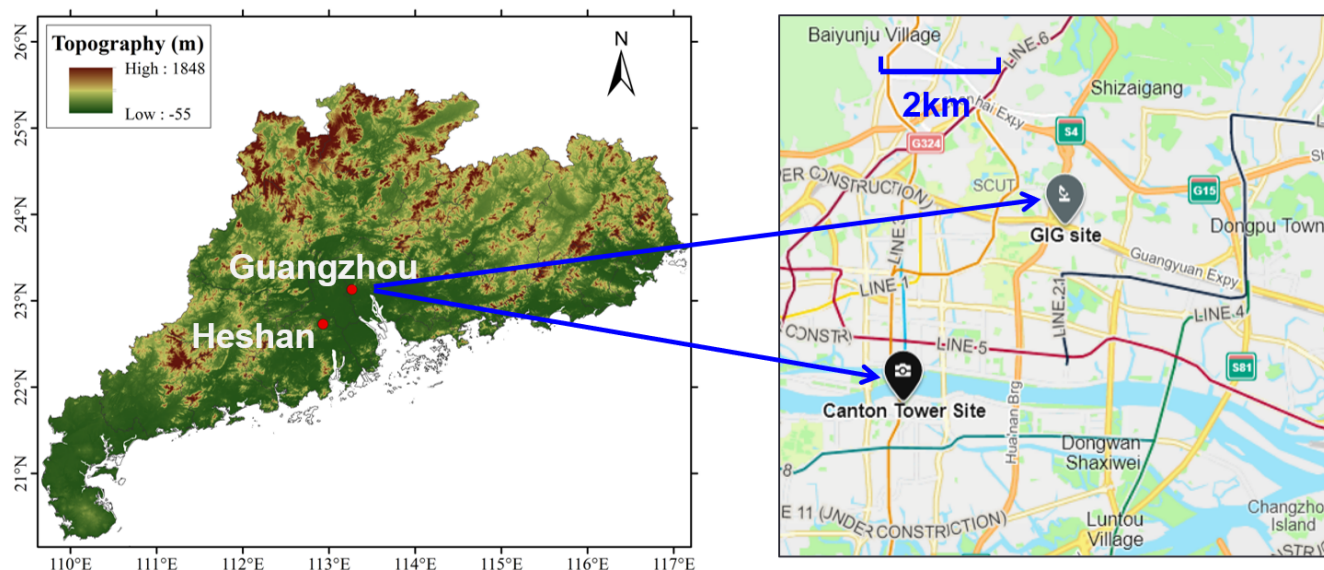
Figure 1. Sampling site at Guangzhou Institute of Geochemistry, Chinese Academy of Sciences (GIG), Heshan and Canton Tower. Note that the map is extracted from © Microsoft Bing maps by the authors.

campaigns. Considering the integrity and temporal coverage of the measurements, we mainly focus on the investigated periods from 7 to 29 October 2018 at the GIG site and from 16 October to 16 November 2019 at the Heshan site.

2.2   Box model description

A zero-dimensional observation-based box model (F0AM) (Wolfe et al., 2016) was used to simulate the production of nitrate in this study. The F0AM box model uses a subset of the Master Chemical Mechanism (MCM) v3.3.1 (Saunders et al., 2003; Jenkin et al., 2003; Bloss et al., 2005), which explicitly describe chemical reactions of VOCs, RO_x radicals (including OH, HO_2 and RO_2), ozone, and nitrate and was widely used in laboratory and theoretical researches (Edwards et al., 2017; Anderson et al., 2017; D'Ambro et al., 2017; Womack et al., 2019).

In this study, the box model was constrained by observations of NMHCs, HCHO, CH_3CHO, NO, CO, CH_4, HONO, and meteorological parameters (i.e., photolysis rates, RH, T, and P) measured at the GIG and Heshan sites. To investigate the convection of nitrate between the residual layer and the surface, the box model was split into two boxes at night (from 17:00 to 06:00 local time (LT) the following morning) to separately represent the nocturnal boundary layer and the residual layer, respectively (Womack et al., 2019) (Fig. S1).

The simulation of the residual layer at the GIG site was constrained by the observation data from 488 m at the Canton Tower, while the simulation of the residual layer at the Heshan site was freely evolved from sunset time using the ground observation data of Heshan. The detailed model settings are described in Sect. S1, and the agreement between

the observation data and simulations at the GIG and Canton Tower sites supports the use of similar simulation of the residual layer at the Heshan site. The model was operated in a time-dependent mode with a 5 min resolution. It was run for a 72 h spin-up time to build steady-state concentrations for secondary pollutants that were not constrained during simulation. To prevent the build-up of long-lived species to unreasonable levels, an additional physical dilution process was applied in the model (Lu et al., 2017; Decker et al., 2019; Novak and Bertram, 2020; Liu et al., 2021; Yun et al., 2018b). To achieve agreement with the observation, lifetimes of 24 and 8 h were used at the GIG and Heshan site, respectively. The sensitivity tests with different dilution constant at the GIG and Heshan site were shown in Figs. S2 and S3, respectively. The background concentrations for ozone and CH_4 were set as 30 ppb and 1.8 ppm, respectively (Wang et al., 2011).

The nocturnal production of nitrate from N_2O_5 hydrolysis and the subsequent Reactions (R5) and (R6) are added to the box model. γ and φ are calculated using the observation-based empirical parameterization method from Yu et al. (2020), where the impacts of nitrate, chloride, and aerosol liquid water content (ALWC) were evaluated to better represent the observed γ. The average values of γ were 0.018 ± 0.01 and 0.019 ± 0.01 at the GIG and Heshan sites, respectively, which were comparable with the observed mean data of γ (0.020 ± 0.019) at the Heshan site in 2017. The φ values used in this study were 0.18 ± 0.15 and 0.20 ± 0.23 at the GIG and Heshan sites, which were slightly lower than the observed mean data of φ at the Heshan site (0.31 ± 0.27) in 2017 (Yu et al., 2020). The chemical compositions of fine particles were not measured at the Canton Tower site, thus

assigned values of γ and φ in the residual layer were equal to those of the nocturnal boundary layer. The γ and φ exhibited complicated nonlinear dependence on aerosol composition, aerosol liquid water, and RH (Bertram and Thornton, 2009; McDuffie et al., 2019; Yu et al., 2020), such that γ and φ have positive and negative dependence with RH, respectively. There was higher RH, and lower chloride at the 488 m site, compared to the ground site of Canton Tower. The nitrate concentration was comparable at the 488 m site to the ground site in the study of Zhou et al. (2020). Combined with the higher RH and lower PM$_{2.5}$ concentrations in the residual layer in this study (as shown in Fig. S4), we inferred the negative deviations for γ and positive deviations for φ in the residual layer. The dry aerosol surface area concentration (S_a) was calculated from the particle number size distribution and calibrated to the actual atmospheric S_a using the RH-dependent hygroscopic growth factor ($f(\text{RH})$). The $f(\text{RH})$ was estimated from the aerosol composition measured by AMS and the aerosol liquid water content, which included the inorganic-associated and organic-associated water. The sum of inorganic-associated water estimated from the ISORROPIA thermodynamic model and organic-associated water estimated from the dry organic aerosol mass was used to calculate the growth of wet matter contributions, as described in the study of McDuffie et al. (2018a). J_{ClNO_2} was scaled from measured NO$_2$ photolysis frequencies divided by a factor of 30 (Riedel et al., 2014).

The equilibrium coefficient between HNO$_3$ and particulate nitrate is incorporated into the box model as a pseudo-first-order reaction (Eqs. 3 and 4) through the equilibrium absorption partitioning theory (Jacob, 2000; Yuan et al., 2016):

$$\text{HNO}_3(\text{g}) \underset{k_{8b}}{\overset{k_{8f}}{\rightleftharpoons}} \text{NO}_3^-(\text{p}), \tag{R8}$$

$$k_{8f} = \left(\frac{R_a}{D_g} + \frac{4}{\omega \cdot \alpha} \right)^{-1} \cdot S_a, \tag{3}$$

$$k_{8b} = \left(\frac{R_a}{D_g} + \frac{4}{\omega \cdot \alpha} \right)^{-1} \frac{S_a}{K_{eq}}, \tag{4}$$

where R_a is the radius of nitrate particles (m), D_g is the gas-phase molecular diffusion coefficient (m^2 s^{-1}), ω is the mean molecular speed of HNO$_3$ (m s^{-1}), α is the mass accommodation coefficient of HNO$_3$, and K_{eq} represents the equilibrium constant of HNO$_3$ and nitrate. These coefficients are the same as those in the chemical aqueous-phase radical mechanism (CAPRAM) (Ervens et al., 2003; Wen et al., 2015).

The empirical kinetic modeling approach (EKMA) is used here to identify the sensitivity of ozone and nitrate to the variations of NO$_x$ and VOCs. The observed diurnal average conditions are used as the input for the base simulation. Sensitivity tests are conducted by increasing and decreasing initial anthropogenic VOCs (AVOCs) and NO$_x$ concentrations by a ratio ranging from 0.1 to 2.0 with 20 equal-distance steps without changing other parameters in the model (Tan et al., 2018; Lyu et al., 2019; Womack et al., 2019). The maximum

concentrations of ozone and nitrate in each scenario are plotted to generate the contour plots of the respective isopleths. Isoprene was included in the simulation as biogenic VOC (BVOC). Reducing BVOCs such as isoprene is impractical, so it is not scaled with AVOC concentrations in the sensitivity simulations on control of precursors.

Since the N$_2$O$_5$ is affected by the chemistry between ozone and VOCs, constraining N$_2$O$_5$ concentrations with the change in NO$_x$ ratio arbitrarily during the isopleth simulations is improper. Thus, we set the simulation of the base case (S0) without N$_2$O$_5$ constrained. To evaluate the results of the base case, we design another simulation with N$_2$O$_5$ constrained (S1) and compare the two simulated nitrate with the observation in Fig. S5. The model scenarios were described in Table S5 in detail. The base case simulation (S0) was comparable to the observation. The simulated nitrate with N$_2$O$_5$ constrained (S1) during 9 to 10 October 2018 was observed to be much higher compared to both the observations and base case simulation (S0) at the GIG site, which suggest that high concentrations of ambient N$_2$O$_5$ measured during this short period may not contribute significantly to nitrate formation (Fig. S6). Overall, the simulated nitrate of the base case without N$_2$O$_5$ constrained agreed well with the observation suggesting the robustness of the model simulations.

Gaussian error propagation was used to evaluate the uncertainties about measurement parameters and reaction rates in the model, as described in Lu et al. (2012). The uncertainties of various measurement parameters (VOC$_S$, trace gases, meteorological parameters, etc.) ranged from 0 % to 20 %, and uncertainties of reaction rates are on the order of ~ 20 % (Lu et al., 2012).

3 Results and discussion

3.1 Overview of nitrate concentrations during the campaign

The temporal variations of mass concentrations of the major chemical components in PM$_1$ are shown in Fig. 2. The mean concentration of PM$_1$ was 41.7 ± 23.1 µg m^{-3} at the GIG site during the investigated period, which was comparable with that at the Heshan site (40.6 ± 15.5 µg m^{-3}). The aerosol composition differed between sites, with inorganic ions (sulfate, nitrate, and ammonia) higher and organic matter lower at the GIG site compared to the Heshan site.

Although the mass concentrations at the two sites were comparable, the mass fraction of nitrate in PM$_1$ at the GIG site increased from 10 % to 33 % as the mass concentration of PM$_1$ increased from 20 to 130 µg m^{-3} (Fig. 3), while the fraction of nitrate increased from 10 % to 20 % at the Heshan site, suggesting that nitrate plays a more important role in the increase in PM$_1$ at the urban site than that at the suburban site. The significant increasing ratio of nitrate fraction from clean conditions to polluted conditions (~ 43 %) was also revealed in the airborne observation in Utah Valley, US
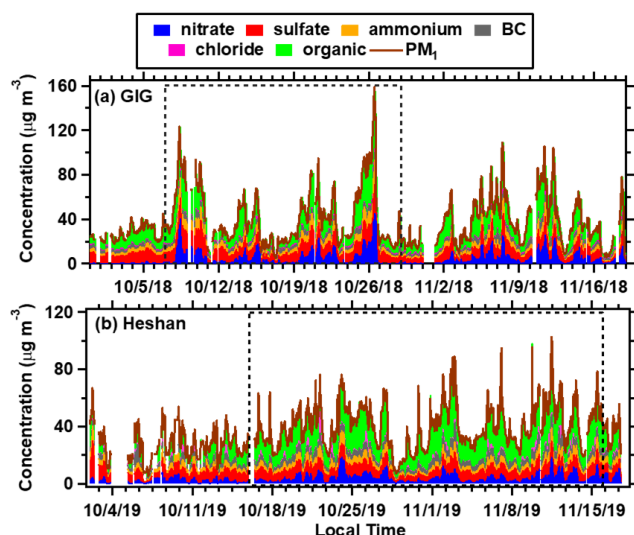
Figure 2. Temporal variations of the mass concentration of the major chemical components in PM_1 including nitrate (NO_3^-), sulfate (SO_4^{2-}), ammonium (NH_4^+), black carbon (BC), chloride (Cl^-), and organics at **(a)** GIG site and **(b)** Heshan site. The black dashed rectangle represents the investigated period which had complete set of data.

Figure 3. The mass concentration ratio of NO_3^- / SO_4^{2-} (top) and fractions of major chemical components (bottom) in PM_1 at **(a)** GIG site and **(b)** Heshan site.

(Franchin et al., 2018). In addition, although the concentration of sulfate was higher than that of nitrate during most of the sampling periods, as PM_1 increased the mass concentration ratio of nitrate / sulfate increased from 0.5 to 2.0 at the GIG site and from 0.5 to 1.5 at the Heshan site. The higher ratios of nitrate / sulfate during the polluted periods imply that reducing nitrate may be essential for reducing the occurrence of PM pollution in southern China. The increasing contributions of nitrate to PM_1 in this study were similar with those observed in northern China during haze pollution (Yang et al., 2017; Fu et al., 2020; Wen et al., 2015; Liu et al., 2015), suggesting the significance of nitrate mitigation to further reduce mass concentrations of fine particles in China.

The diurnal patterns of mean nitrate, NH_3, NO_2, and HNO_3 concentrations observed at the GIG and Heshan sites are shown in Fig. 4. The highest nitrate concentration was observed in the morning at the GIG site and during nighttime at the Heshan site, suggesting differences in the processes that dominated the formation of nitrate at the two sites. At the GIG site, nitrate rapidly increased from 04:00 to 09:00 LT, but the concentrations of NH_3 and HNO_3 increased slowly, which suggests the minor contribution of direct production of HNO_3 from the reaction of OH and NO_2. The increase in nitrate during this period might be associated with the downward transport from the residual layer to the ground. The diurnal variations in O_3 and NO_x measured at the GIG and Canton Tower sites are shown in Fig. 5. The ground-based observations at the Canton Tower showed similar variation patterns of O_3 and NO_x to the GIG site. However, the average concentration of O_3 at 488 m of Canton Tower site was
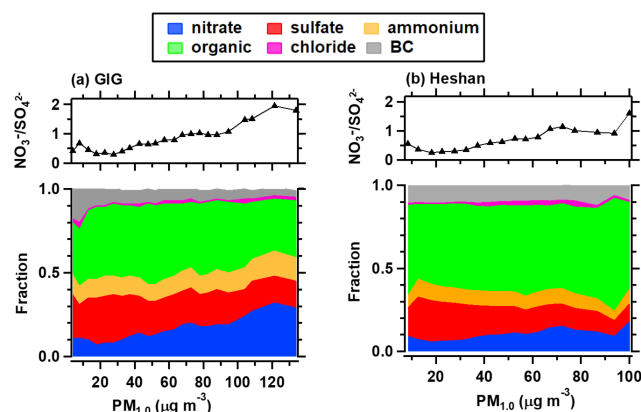
2.4 times higher than that at the GIG site during nighttime, and the lower nocturnal concentrations of NO (nearly zero) at the 488 m site would enhance the production of NO_3 and N_2O_5 (Wang et al., 2018b; McDuffie et al., 2019). Therefore, heterogeneous uptake of N_2O_5 during nighttime may be active at 488 m at the urban site, which will be further investigated in Sect. 3.2. At the Heshan site, nitrate increased sharply in the early nighttime (before midnight), which may be attributable to the shallow nocturnal boundary layer or the enhanced nocturnal N_2O_5 heterogeneous uptake reactions. Subsequently, there was a significant increase in nitrate from 07:00 to 09:00 LT. The concentration of NH_3 showed a variation pattern that was similar to that of nitrate and increased after 07:00 LT, while the concentrations of HNO_3 and NO_2 showed a decreasing trend from 07:00 to 09:00 LT at the Heshan site. The different growth characteristics of nitrate and the variation patterns of precursors at the two sites may be related to different formation processes, which will be discussed in detail later.

In this study, the wind speeds in the investigated periods at the GIG and Heshan sites were generally below $2\,m\,s^{-1}$ (Table S6), which suggests that regional transport may have limited contributions to the abundance of nitrate at the observation sites. Therefore, the discussion of the chemical formation process of nitrate in this study focuses on local production.

The molar ratios of $[NH_4^+]$ to the sum of $2 \times [SO_4^{2-}] + [NO_3^-]$ are calculated (Fig. S7) to determine whether there was enough NH_4^+ to neutralize nitrate. The molar ratios were approximately 1.0 at both GIG and Heshan sites, suggesting both NH_3 and HNO_3 were crucial precursors for nitrate formation. Based on these discussions, we will discuss the NH_3 effect on the nitrate partitioning firstly using the thermodynamic ISORROPIA II model (Fountoukis et al., 2007). The nitrate chemical formation pathways, which are mainly attributable to the production of
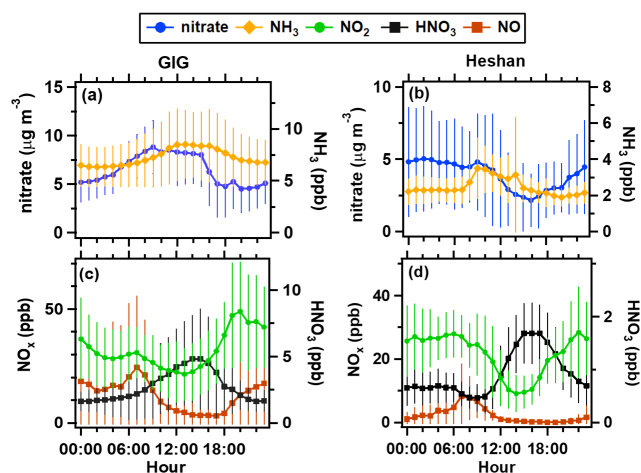
Figure 4. Diurnal variations of mean concentrations of nitrate and related pollution species at **(a)** GIG site and **(b)** Heshan site. The error bars represent the standard deviation of the means.

HNO$_3$ and/or heterogeneous uptake of N$_2$O$_5$ combining the box model, will be discussed in Sect. 3.2.

The ISORROPIA II model setting is described in Sect. S2 in detail. The ISORROPIA II modeled results of nitrate, ammonium, HNO$_3$, and NH$_3$ at the GIG and Heshan sites were displayed in Figs. S8–S9. The particle-phase nitrate and ammonium at the GIG site showed a slight overestimation, while the gas-phase HNO$_3$ and NH$_3$ showed overestimation at the Heshan site. Overall, the simulated components showed good correlations with the observed concentrations at both sites. We use the ISORROPIA II model results to evaluate the particle fraction of nitrate in the sum of HNO$_3$+nitrate ($\varepsilon(NO_3^-)$) against aerosol pH. Aerosol pH, which depends on the aerosol acidity and water content, is calculated by the following equation:

$$pH = -\log_{10} \frac{1000 H_{air}^+}{ALWC},$$ (5)

where H_{air}^+ ($\mu g\,m^{-3}$) is the hydronium concentration of the equilibrium particle and ALWC ($\mu g\,m^{-3}$) is the aerosol water content from ISORROPIA II simulation.

The $\varepsilon(NO_3^-)$ against pH at the GIG and Heshan sites are shown in Fig. 6. The pH data are colored by relative humidity and fit to an "s curve" as in Guo et al. (2018). The clustering of pH data mainly located between 1–3 and the $\varepsilon(NO_3^-)$ are sensitive to the change of pH. To further evaluate the sensitivity of NH$_3$ and sulfate on this effect, the input of total ammonium (NH$_x$, ammonium + NH$_3$) and sulfate were reduced from 10 % to 90 % relative to the ISORROPIA II base model, respectively, while keeping other parameters constant. The response of simulated nitrate concentration and aerosol pH to changes in NH$_x$ and SO$_4^{2-}$ are shown in Fig. 7. The nitrate concentration decreased with the reduction of NH$_x$ and had little variation with the reduction of SO$_4^{2-}$ (Fig. 7a–b)

at both sites. Along with the reduction of NH$_x$, the pH values decreased significantly (Fig. 7c–d), which caused the further decrease in $\varepsilon(NO_3^-)$. The pH values showed a slight increase with the reduction of SO$_4^{2-}$, which may be caused by there being more available ammonium to neutralize the hydronium. It is consistent with the study of Guo et al. (2018) and Nenes et al. (2020), suggesting the partitioning of nitrate was also affected by the NH$_3$ in the pH values between 1–3. Thus, the control of NH$_3$ is effective for the reduction of nitrate by affecting the partitioning process of nitrate at both GIG and Heshan sites in this study. The partitioning of nitrate increased with the reduction of sulfate suggests the limited role of sulfate reduction on the mitigation of nitrate.

3.2 Contributions of different pathways to nitrate formation

To further investigate the chemical formation pathways of nitrate, which related to the photochemical and heterogeneous reactions, we adopt the box model results to simulate the contribution of different pathways to nitrate formation. The temporal variations in simulated and observed nitrate concentrations at the GIG and Heshan sites are presented in Fig. 8; simulated and observed nitrate showed similar concentrations and variation patterns. The diurnal variation of simulated nitrate is compared with the observation in Fig. S10. The diurnal simulated nitrate was comparable with the observation at the GIG site, especially when considering the vertical transport from the residual layer in the morning. Unlike the GIG site, the diurnal simulated nitrate was higher in the daytime, and a little bit lower in the late nighttime, compared with the observation at the Heshan site. It may be related to the lack of quantitative transport in the box model. The box model performance was evaluated using the mean bias (MB), index of agreement (IOA), and correlation coefficient (r) (Table S7) (X. Liu et al., 2019; Lyu et al., 2017; Wang et al., 2019; Curci et al., 2015). The IOA was larger than 0.7 and r was larger than 0.5 at both sites, indicating good agreements between simulated and observed nitrate concentrations. The temporal variations in simulated N$_2$O$_5$ and ClNO$_2$ concentrations were higher than the observations at the Heshan site as shown in Fig. S6c, d, and the simulated results at the GIG site from 9 to 10 October were significantly lower than the observations (Fig. S6a, b). The abnormally high observed concentrations of N$_2$O$_5$ and ClNO$_2$ that lasted for short periods (10–30 min) at the GIG site may be caused by transported air masses from upwind regions or vertical transport without well-mixed and with fresh urban NO emissions. Simulation of these near-instantaneous processes transported to the site using a box model is difficult, as a box model is more suitable to simulate the well-mixed air mass with few transport effects. However, the simulated nitrate concentrations without observed N$_2$O$_5$ constrained was adequately comparable with the observations as shown in Fig. S5, implying the in-
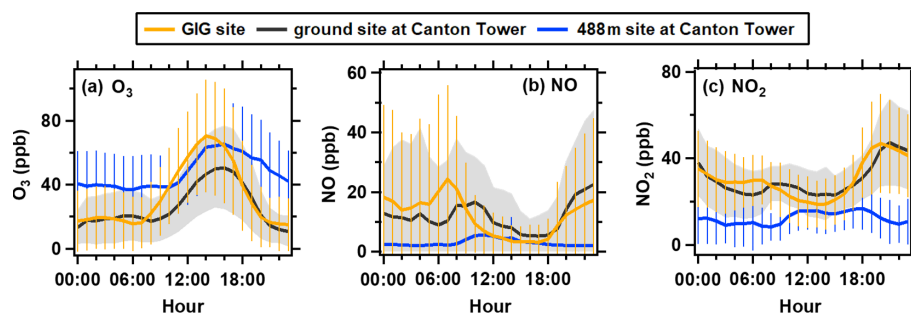
Figure 5. Diurnal variation of mean concentrations of **(a)** O_3, **(b)** NO, **(c)** NO_2 at GIG (orange lines), and the ground and 488 m sites of Canton Tower (black and blue lines, respectively). The orange and blue error bars represent the standard deviations of the mean concentrations at the GIG site and the 488 m site of Canton Tower; the grey areas show 1 standard deviation of the mean concentration at ground site of Canton Tower.
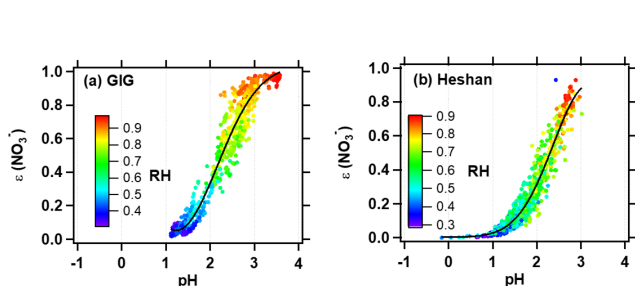

Figure 6. The particle fraction of nitrate in the sum of $HNO_3 +$ nitrate ($\varepsilon(NO_3^-)$) against aerosol pH. The pH data are colored by relative humidity and fit to an "s curve" in black line, as shown in Guo et al. (2018).
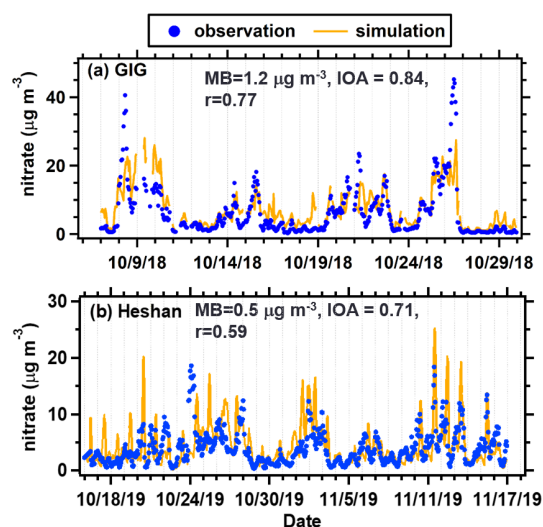
Figure 8. Comparison of the temporal box model simulated and observed nitrate at the **(a)** GIG site and **(b)** Heshan site.
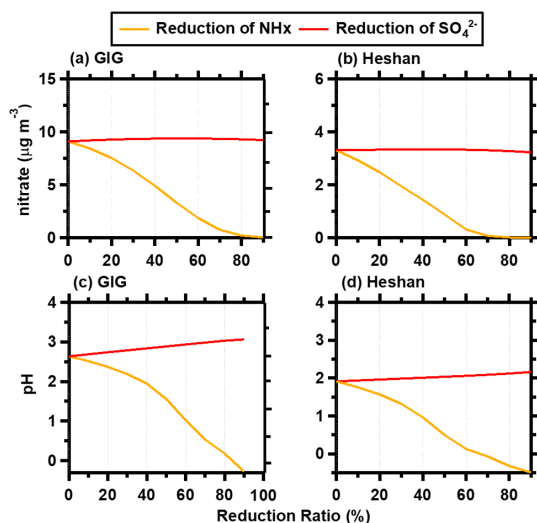
Figure 7. ISORROPIA-predicted average nitrate **(a, b)** and pH **(c, d)** as a function of changes in NH_x (ammonium $+ NH_3$, orange line) and SO_4^{2-} (red line) at the GIG and Heshan site during the study period.

fluence of the instantaneously high concentrations of N_2O_5 on nitrate formation was negligible at the GIG site.

Based on these simulation results, we calculated the daily-averaged contributions of the two different reaction pathways to the nitrate concentration – the daytime production from $OH + NO_2$ reaction and the nighttime production from N_2O_5 uptake reaction in the nocturnal boundary layer and in the residual layer. The nitrate produced in the residual layer is only gradually mixed to the surface as the boundary layer develops during the following morning, while the nitrate contributed to the boundary layer column concentration always included the N_2O_5 uptake in the residual layer during the whole nighttime (Wang et al., 2018a; Womack et al., 2019). The calculation methods to determine contribution to the boundary layer column concentrations and to ground-level nitrate concentrations should be distinguished.

To calculate the contribution to the boundary layer column concentration, the integral of the nitrate production rate from

N_2O_5 uptake from both the nocturnal surface layer and the residual layer directly contribute to nitrate column concentrations layer during the whole nighttime, weighted as 0.4 and 0.6 based on their altitude fractions of the two layers, respectively. This calculation for the contributions to column concentration is the same as the methods presented by Wang et al. (2018a) and Womack et al. (2019). However, to quantify the contribution of nitrate produced from the residual layer to the ground nitrate concentration, one must account for the dynamic exchange between the residual layer and the surface-based boundary layer that develops during daytime. The integral time for this dynamic exchange was assumed to be from 06:00 to 10:00 LT in the morning. Detailed descriptions of the calculations are provided in Sect. S3 in the Supplement. The calculation about partitioning processes from OH and NO_2 reaction in the daytime was the same in the two methods mentioned above, which was the partition part of the integral of the OH and NO_2 reaction during the daytime.

The contributions of nitrate to the boundary layer column concentration (i.e., average from ground to 1000 m) are shown in Fig. 9a. The contribution of the nitrate production rate from N_2O_5 uptake in the residual layer was 17.9 µg m^{-3} d^{-1} at the GIG site, which was much greater than the N_2O_5 uptake in the nocturnal boundary layer (0.4 µg m^{-3} d^{-1}). This may be caused by the fresh NO surface emissions, which titrate the NO_3 radical and ozone in the nocturnal boundary layer, as the mean NO concentration during the nighttime at the GIG site was 12.1 ppb. The contribution from nocturnal nitrate production in the boundary layer was comparable with the contribution from OH and NO_2 reaction (13.2 µg m^{-3} d^{-1}) during the daytime. In contrast to the GIG site, the contribution of the nitrate production rate from N_2O_5 uptake in the nocturnal boundary layer (6.2 µg m^{-3} d^{-1}) was comparable with that in the residual layer (4.4 µg m^{-3} d^{-1}) at the Heshan site. The similar nitrate concentration and production rate from N_2O_5 uptake between the nocturnal boundary layer and residual layer in Fig. S12c, d was due to lower NO emissions at the Heshan site. The results demonstrate that nocturnal nitrate production plays an important role in nitrate production in the boundary layer, with nighttime contributions of 58 % at the urban site and 35 % at the suburban site.

The relative magnitudes of the contributions to the daily-averaged surface nitrate differ somewhat from the contributions to the entire boundary layer. The contributions from the three major pathways to surface nitrate concentrations at the two sites are compared in Fig. 9b. At the GIG site the nitrate production rate from the OH and NO_2 reaction and downward transport from the residual layer were 13.2 and 16.6 µg m^{-3} d^{-1}, contributing 43 % and 53 % of ground-level nitrate concentrations, with a minor contribution (1.1 µg m^{-3} d^{-1}) from the production of N_2O_5 uptake in the nocturnal boundary layer. This is similar with the results in Fig. 9a, implying a large nitrate contribution from N_2O_5
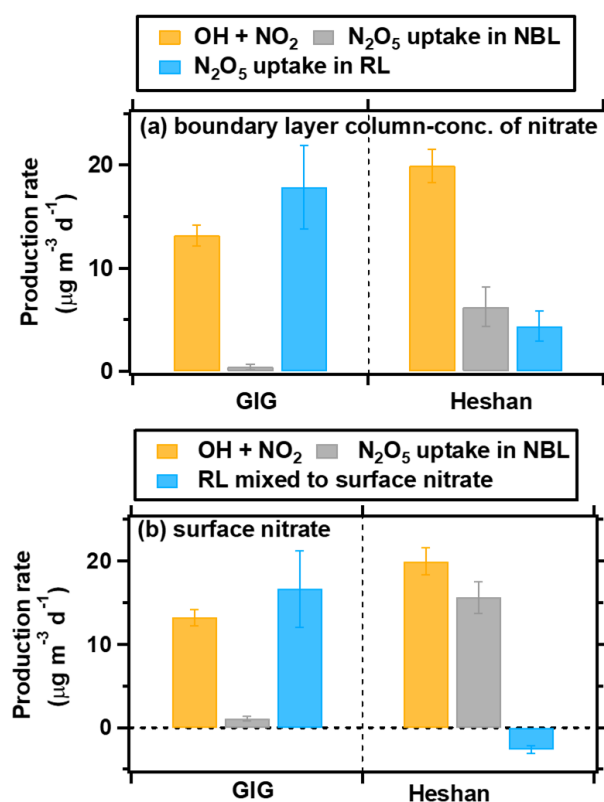

Figure 9. The daily-averaged contribution **(a)** to boundary layer column concentration and **(b)** to surface nitrate from three pathways (OH + NO_2 reaction, N_2O_5 uptake in NBL, and N_2O_5 uptake in RL or N_2O_5 uptake from RL mixed process) at the GIG and Heshan sites. The error bars represent the standard deviations of the mean production rate.

uptake in the residual layer, but not in the nocturnal boundary layer at the urban site.

However, at the suburban Heshan site (Fig. 9b), downward transport from the residual layer made no contribution to the surface nitrate concentration, which was smaller than the contribution of nitrate from the residual layer in Fig. 9a. This is due to the similar nitrate production rate from N_2O_5 uptake between the nocturnal boundary layer and residual layer (see Fig. S12), inducing negligible convection between the two layers as the result of small concentration gradient (Brown et al., 2003; Baasandorj et al., 2017; Prabhakar et al., 2017). The nitrate production rate from OH and NO_2 reaction (19.9 µg m^{-3} d^{-1}) and nocturnal N_2O_5 uptake (15.6 µg m^{-3} d^{-1}) were the major nitrate formation pathways, which contributed 56 % and 44 % to the surface total nitrate production, respectively. Therefore, the importance of residual layer contribution to the surface nitrate can vary significantly and should be comprehensively evaluated in different environments. In addition, the nitrate contributions to the surface concentrations and boundary layer column con-

centrations can also be different in different regions, which should be clarified and distinguished in future studies.

In summary, the N_2O_5 uptake reaction was active in the residual layer both at urban and suburban sites, and the downward transport from the residual layer was a significant contributor to surface nitrate at the urban site, but not at the suburban site. This is attributable to the titration of the NO_3 radical and ozone by fresh NO emissions during the stagnant boundary layer at the urban site, resulting in the large difference of nitrate production between the residual and nocturnal boundary layers. In contrast, at the suburban site, lower NO emissions favored NO_3 production and heterogeneous uptake of N_2O_5 both in the nocturnal boundary layer and the residual layer. The horizontal transport in the residual layer from nocturnal jets may contribute to the different nitrate production at urban and suburban sites, which has been discussed in the research of Chow et al. (2006) and Brown et al. (2006). Due to the limitation of the box model, this issue could be studied by the chemistry transport model in further research.

3.3   Control of NO_x and VOCs as mitigation strategies of nitrate

Overall, the contributions of nitrate from the three major pathways, all involving NO_x and ozone, suggest that nitrate formation depends not only on the reactions of NO_x but also is closely associated with the VOC–NO_x–O_3 chemistry. Therefore, the influence of both NO_x and VOC reduction on nitrate production should be considered in formulating policies to control aerosol pollution.

In this study, we adopted the widely used EKMA approach, generally used for ozone sensitivity analysis (Edwards et al., 2014; Mazzuca et al., 2016; Xue et al., 2014b; Wang et al., 2015) to investigate the response of nitrate formation in changing emissions of VOCs and NO_x. The dependence of simulated nitrate concentrations on the changing of VOC and NO_x concentration allows the construction of isopleths of nitrate and ozone production at the GIG and Heshan sites, as displayed in Fig. 10. The production of nitrate and ozone were in the VOC-limited regime at the GIG site, and in the transition regime at the Heshan site, where nitrate and ozone are sensitive to both VOCs and NO_x reduction. As shown in Fig. 11, the reduction of NO_x emissions from 0 %– 70 % would increase nitrate and ozone concentrations at the GIG site but decrease those concentrations at the Heshan site. The decrease in VOC concentrations would decrease nitrate and ozone concentrations at both sites. These results suggest that control of VOC emissions will efficiently reduce nitrate and ozone production in both urban and suburban areas, but control of NO_x emissions will give different responses between urban and suburban area for both ozone and nitrate. Figure 11 shows that the nitrate sensitivity to the reduction of VOCs and NO_x emissions was identical to the response of ozone at both sites. These results demonstrate the possibility
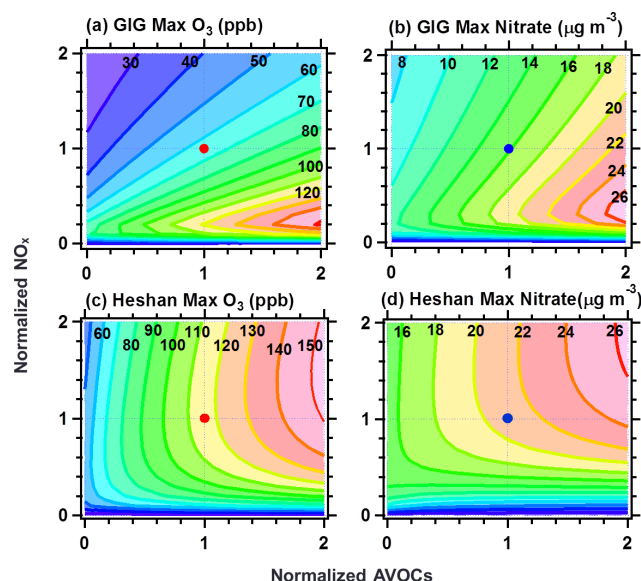

Figure 10. The simulated isopleths of ozone and nitrate with normalized NO_x and AVOCs concentration at the **(a, b)** GIG site and **(c, d)** Heshan site, each isopleth represents the maximum ozone and nitrate in the simulation, and the red and blue circles represent the base cases.
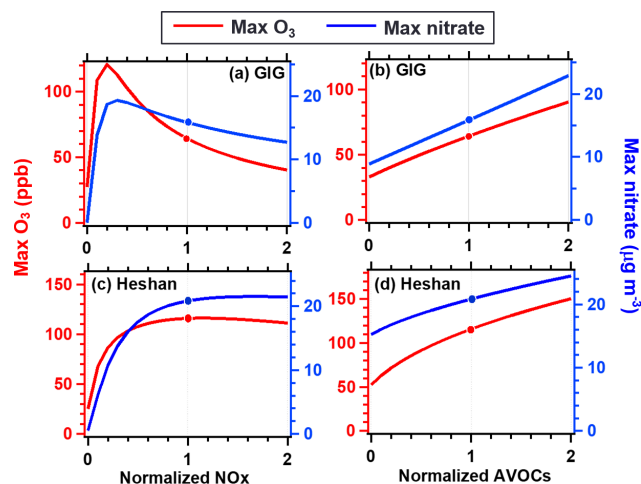

Figure 11. Simulated maximum ozone and nitrate concentration with normalized NO_x and AVOCs at the **(a, b)** GIG site and **(c, d)** Heshan site, cutting through the simulated isopleth in Figure 8 with normalized AVOCs and NO_x ratio at 1, respectively. The red and blue circles represent the base cases.

of synergetic control for nitrate and ozone at both urban and suburban sites through VOC control.

The accuracy of the isopleth plots in Fig. 10 depends on several variables and parameters included in the box model. Figures S13–S14 show the results of simulation experiments on the dependence of the isopleths upon changing various parameterization for estimating HONO concentrations, N_2O_5 uptake coefficient, and $ClNO_2$ yields as described in Sect. S4.

The sensitivity regime of nitrate and ozone did not change, although the peak concentrations of ozone and nitrate did change, which supports the reliability of the results discussed above.

As nitrate and ozone exhibit similar sensitivity to the reduction of NO_x and VOCs, different VOCs / NO_x ratios may point to different control strategies. In the cases of the Heshan and GIG sites, the reduction of NO_x can adequately control nitrate production with a VOCs / NO_x ratio of 1.8 at the Heshan site, while a contrary result can be found at the GIG site (with a VOCs / NO_x ratio of 0.8) with a less than 70 % reduction of NO_x emission. The simulated results at the GIG site agree well with those reported in the urban areas of Shanghai in China (Dong et al., 2014) and the Salt Lake City and San Joaquin Valley in the US (Betty and Christian, 2001; Womack et al., 2019), which all emphasized the decrease in nitrate production with the reduction of VOC emissions, and the enhanced nitrate production with NO_x reduction. The results at the Heshan site were consistent with the simulations at the suburban site of northern China, where a higher VOC / NO_x ratio was found (Wen et al., 2018; Lu et al., 2019). The synergetic reduction of NO_x and VOCs is necessary to effectively mitigate the nitrate production in consideration of the different VOC / NO_x ratios in the urban and suburban areas.

The above discussions revealed that direct reduction of NO_x may not lead to a decrease in nitrate production. Meanwhile, the reduction of VOCs is effective to mitigate nitrate production, though they were not the direct precursors of nitrate. To illustrate these findings, the impacts of changing VOCs and NO_x on the production rate of the OH radical, the rate of OH plus NO_2, and the N_2O_5 uptake reaction were evaluated. During daytime nitrate production involves OH production and its subsequent reaction with NO_2. As shown in Fig. 12, the NO_x-saturated condition at the GIG site provided sufficient NO_2 to quench the OH radical during daytime. A less than 70 % reduction of NO_x will increase ozone production and thereby drive more production of OH, leading to increase in the OH and NO_2 reaction rates. When NO_x is lower than 30 % of the base case emissions, ozone production would decrease and lead to the decrease in OH production and its reaction with NO_2, which in turn bring about a decrease in nitrate production. In contrast, at the Heshan site, the base case NO_x concentrations are lower, giving a production rate of OH that is already sensitive to both NO_x and VOC reductions. The model results indicate that further emission reductions in both NO_x and VOCs will simultaneously mitigate the production of nitrate and ozone.

During nighttime, the initial ozone concentration participated the nocturnal chemistry increased (decreased) with the reduction of NO_x at the GIG (Heshan) site. In addition, the decrease in NO_x will reduce the titration effect of NO on NO_3 radical and ozone at the GIG site, which enhances production of N_2O_5 and promotes nitrate production in both the nocturnal boundary layer and the residual layer (Fig. 13).
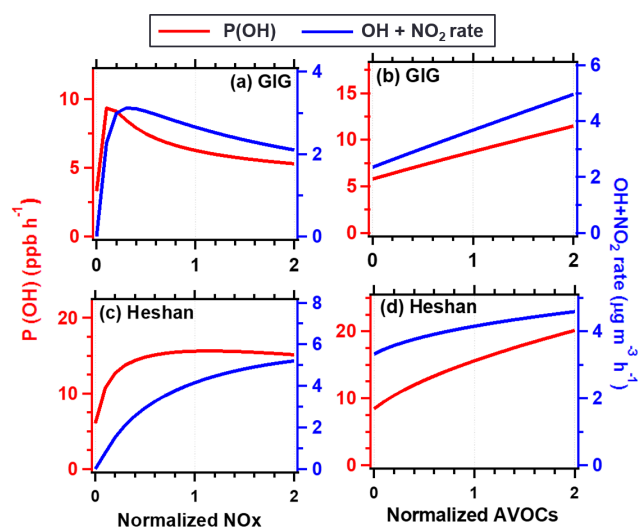

Figure 12. Simulated average production rates of OH (P (OH)) and the reaction rate of OH and NO_2 with the normalized changes of NO_x and AVOC emissions at the (a, b) GIG site and (c, d) Heshan site.
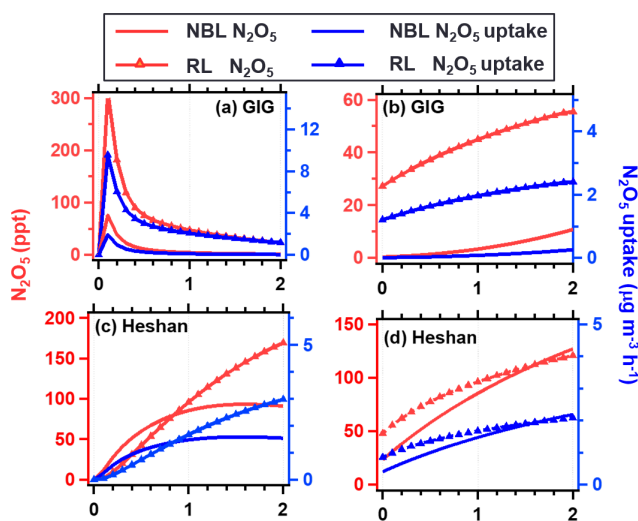

Figure 13. Simulated average concentration of N_2O_5 and nitrate production rate from N_2O_5 uptake with the normalized changes of NO_x and AVOC emissions at the (a, b) GIG site and (c, d) Heshan site in the NBL and RL.

However, at the Heshan site, the reduction of NO_x cuts down the sources of NO_2 and NO_3, decreasing the formation of N_2O_5 and thus its heterogeneous uptake to produce nitrate. The reduction of VOCs decreases ozone formation during daytime, thus attenuating the nocturnal formation of NO_3, N_2O_5, and nitrate at both the GIG and Heshan sites.

In summary, nitrate and ozone show similar responses to the reduction of NO_x and VOCs for both daytime and nighttime chemical processes, as the result of the coupling between the formation reactions of ozone and nitrate. The re-

sults of this study emphasize the complex effects of reductions of NO_x emissions on nitrate concentrations in the urban and suburban areas. In addition, the reduction of VOC emissions would be effective in the concurrent mitigation of ozone and nitrate, suggesting that the reduction of VOCs at present is an effective method for the synergistic control of ozone and $PM_{2.5}$ at present. As there are limitations of box modeling, a comprehensive three-dimensional model assessment is needed on a regional scale.

4   Conclusions

In this study, we use an observation-constrained box model to explore the nitrate formation pathways and implications for nitrate mitigation strategies at urban and suburban sites. At both sites, the mass fraction of nitrate in PM_1 increased as the absolute PM_1 levels increased (from 10 % to 33 % at the urban site and from 10 % to 20 % at the suburban site), suggesting the important role played by nitrate in increasing particle concentrations in the PRD.

Both HNO_3 and NH_3 are important precursors for nitrate formation. Combined with the ISORROPIA II thermodynamic model, the reduction of NH_3 is effective for the nitrate reduction by affecting the partitioning process of nitrate at both GIG and Heshan sites. The box model simulations demonstrate that chemical reactions in the daytime and at night both contributed significantly to formation of nitrate in the boundary layer at the two sites, with nighttime contributions of 58 % at the urban site and 35 % at the suburban site. However, nighttime reactions predominantly occurred aloft in the residual layer at the urban site, and downward transport from the residual layer in the morning is an important source (53 %) for surface nitrate at the urban site, whereas similar amounts of nitrate were produced in the nocturnal boundary layer and residual layer at the suburban site, which results in little downward transport of nitrate from the residual layer to the ground at this region. The spatial differences of nocturnal reactions and the different contributions from downward transport of the residual layer to surface nitrate at urban and suburban sites were attributed to different fresh emissions and concentration levels of NO_x at the two sites during the nighttime, suggesting that nitrate production under different NO_x conditions should be explored to better understand the its formation pathways.

The non-linear relationships between nitrate, NO_x, and VOCs were developed to investigate the nitrate mitigation strategies. The simulations demonstrated that the formation processes of both nitrate and ozone were in the VOC-limited region at the urban site and in the transition region at the suburban site. The same sensitivity regimes of nitrate and ozone at two sites was caused by the similar chemical processes that combine to produce nitrate and ozone. These results suggest that control of VOC emissions would effectively mitigate nitrate in both urban and suburban areas.

Overall, the formation processes of nitrate are systematically investigated in both urban and suburban areas in this study, which provides the opportunity to identify different influencing factors of nitrate production in different environments and offers insights into the comprehensive mitigation of nitrate pollution in regional scale. NO_x emission controls alone might not be an effective strategy for reducing the nitrate production, while the reduction of VOC emissions would take effect in the concurrent mitigation of ozone and nitrate. Thus, an emission control policy focusing on VOCs will be an effective means for the synergistic control of ozone and $PM_{2.5}$ at present. In the long-term, multi-pollutant control should be implemented to achieve better control strategies for ozone and $PM_{2.5}$. As the result of limitation for the 0-D box model, vertical transport and horizontal transport cannot be considered explicitly in this study. Given the limitations of the box model, three-dimensional models should be used to further investigate the synergistic control of ozone and particles on the regional scale.

Author contributions. BY and MS designed the research. SXY, YWP, SH, WC, WWH, CLP, CMW, ZLW, TGL, EZ, MFC, XBL, SHW, CHW, JPQ, WBL, CW, WJW, CSY, WS, and PC contributed to data collection. SXY performed the data analysis, with contributions from JZ, DDP, XJH, CCL, XYY, YS, HCW, DHC, XuW, ZYZ, JYZ, and XiW. SXY and BY prepared the paper with contributions from the other authors. All the authors reviewed the paper.

Review statement. This paper was edited by Kostas Tsigaridis and reviewed by four anonymous referees.

References

Anderson, D. C., Nicely, J. M., Wolfe, G. M., Hanisco, T. F., Salawitch, R. J., Canty, T. P., Dickerson, R. R., Apel, E. C., Baidar, S., Bannan, T. J., Blake, N. J., Chen, D., Dix, B., Fernandez, R. P., Hall, S. R., Hornbrook, R. S., Gregory Huey, L., Josse, B., Jöckel, P., Kinnison, D. E., Koenig, T. K., Le Breton, M., Marécal, V., Morgenstern, O., Oman, L. D., Pan, L. L., Percival, C., Plummer, D., Revell, L. E., Rozanov, E., Saiz-Lopez, A., Stenke, A., Sudo, K., Tilmes, S., Ullmann, K., Volkamer, R., Weinheimer, A. J., and Zeng, G.: Formaldehyde in the Tropical Western Pacific: Chemical Sources and Sinks, Convective Transport, and Representation in CAM-Chem and the CCMI Models, J. Geophys. Res.-Atmos., 122, 11201–211226, https://doi.org/10.1002/2016JD026121, 2017.

Baasandorj, M., Hoch, S. W., Bares, R., Lin, J. C., Brown, S. S., Millet, D. B., Martin, R., Kelly, K., Zarzana, K. J., Whiteman, C. D., Dube, W. P., Tonnesen, G., Jaramillo, I. C., and Sohl, J.: Coupling between Chemical and Meteorological Processes under Persistent Cold-Air Pool Conditions: Evolution of Wintertime $PM_{2.5}$ Pollution Events and N_2O_5 Observations in Utah's Salt Lake Valley, Environ. Sci. Technol., 51, 5941–5950, https://doi.org/10.1021/acs.est.6b06603, 2017.

Bertram, T. H. and Thornton, J. A.: Toward a general parameterization of N_2O_5 reactivity on aqueous particles: the competing effects of particle liquid water, nitrate and chloride, Atmos. Chem. Phys., 9, 8351–8363, https://doi.org/10.5194/acp-9-8351-2009, 2009.

Betty, P. and Christian: Sensitivity of particulate matter nitrate formation to precursor emissions in the California San Joaquin Valley, Environ. Sci. Technol., 35, 2979–2987, 2001.

Bian, H., Chin, M., Hauglustaine, D. A., Schulz, M., Myhre, G., Bauer, S. E., Lund, M. T., Karydis, V. A., Kucsera, T. L., Pan, X., Pozzer, A., Skeie, R. B., Steenrod, S. D., Sudo, K., Tsigaridis, K., Tsimpidi, A. P., and Tsyro, S. G.: Investigation of global particulate nitrate from the AeroCom phase III experiment, Atmos. Chem. Phys., 17, 12911–12940, https://doi.org/10.5194/acp-17-12911-2017, 2017.

Bloss, C., Wagner, V., Jenkin, M. E., Volkamer, R., Bloss, W. J., Lee, J. D., Heard, D. E., Wirtz, K., Martin-Reviejo, M., Rea, G., Wenger, J. C., and Pilling, M. J.: Development of a detailed chemical mechanism (MCMv3.1) for the atmospheric oxidation of aromatic hydrocarbons, Atmos. Chem. Phys., 5, 641–664, https://doi.org/10.5194/acp-5-641-2005, 2005.

Brown, S. G., Hyslop, N. P., Roberts, P. T., McCarthy, M. C., and Lurmann, F. W.: Wintertime Vertical Variations in Particulate Matter (PM) and Precursor Concentrations in the San Joaquin Valley during the California Regional Coarse PM/Fine PM Air Quality Study, J. Air Waste Manage., 56, 1267–1277, https://doi.org/10.1080/10473289.2006.10464583, 2006.

Brown, S. S., Stark, H., Ryerson, T. B., Williams, E. J., Nicks Jr., D. K., Trainer, M., Fehsenfeld, F. C., and Ravishankara, A. R.: Nitrogen oxides in the nocturnal boundary layer: Simultaneous in situ measurements of NO_3, N_2O_5, NO_2, NO, and O_3, J. Geophys. Res.-Atmos., 108, 4299, https://doi.org/10.1029/2002jd002917, 2003.

Chen, W., Ye, Y., Hu, W., Zhou, H., Pan, T., Wang, Y., Song, W., Song, Q., Ye, C., Wang, C., Wang, B., Huang, S., Yuan, B., Zhu, M., Lian, X., Zhang, G., Bi, X., Jiang, F., Liu, J., Canonaco, F., Prevot, A. S. H., Shao, M., and Wang, X.: Real-time characterization of aerosol compositions, sources and aging processes in Guangzhou during PRIDE-GBA 2018 campaign, J. Geophys. Res.-Atmos., 126, e2021JD035114, https://doi.org/10.1029/2021JD035114, 2021.

Chen, X., Wang, H., Lu, K., Li, C., Zhai, T., Tan, Z., Ma, X., Yang, X., Liu, Y., Chen, S., Dong, H., Li, X., Wu, Z., Hu, M., Zeng, L., and Zhang, Y.: Field Determination of Nitrate Formation Pathway in Winter Beijing, Environ. Sci. Technol., 54, 9243–9253, https://doi.org/10.1021/acs.est.0c00972, 2020.

Chow, J. C., Chen, L. W. A., Watson, J. G., Lowenthal, D. H., Magliano, K. A., Turkiewicz, K., and Lehrman, D. E.: $PM_{2.5}$ chemical composition and spatiotemporal variability during the California Regional $PM_{10}/PM_{2.5}$ Air Quality Study (CRPAQS), J. Geophys. Res.-Atmos., 111, D10S04, https://doi.org/10.1029/2005JD006457, 2006.

Curci, G., Ferrero, L., Tuccella, P., Barnaba, F., Angelini, F., Bolzacchini, E., Carbone, C., Denier van der Gon, H. A. C., Facchini, M. C., Gobbi, G. P., Kuenen, J. P. P., Landi, T. C., Perrino, C., Perrone, M. G., Sangiorgi, G., and Stocchi, P.: How much is particulate matter near the ground influenced by upper-level processes within and above the PBL? A summertime case study in Milan (Italy) evidences the distinctive role of nitrate, Atmos. Chem. Phys., 15, 2629–2649, https://doi.org/10.5194/acp-15-2629-2015, 2015.

D'Ambro, E. L., Møller, K. H., Lopez-Hilfiker, F. D., Schobesberger, S., Liu, J., Shilling, J. E., Lee, B. H., Kjaergaard, H. G., and Thornton, J. A.: Isomerization of Second-Generation Isoprene Peroxy Radicals: Epoxide Formation and Implications for Secondary Organic Aerosol Yields, Environ. Sci. Technol., 51, 4978–4987, https://doi.org/10.1021/acs.est.7b00460, 2017.

Decker, Z. C. J., Zarzana, K. J., Coggon, M., Min, K.-E., Pollack, I., Ryerson, T. B., Peischl, J., Edwards, P., Dubé, W. P., Markovic, M. Z., Roberts, J. M., Veres, P. R., Graus, M., Warneke, C., de Gouw, J., Hatch, L. E., Barsanti, K. C., and Brown, S. S.: Nighttime Chemical Transformation in Biomass Burning Plumes: A Box Model Analysis Initialized with Aircraft Observations, Environ. Sci. Technol., 53, 2529–2538, https://doi.org/10.1021/acs.est.8b05359, 2019.

Dong, H.-B., Zeng, L.-M., Hu, M., Wu, Y.-S., Zhang, Y.-H., Slanina, J., Zheng, M., Wang, Z.-F., and Jansen, R.: Technical Note: The application of an improved gas and aerosol collector for ambient air pollutants in China, Atmos. Chem. Phys., 12, 10519–10533, https://doi.org/10.5194/acp-12-10519-2012, 2012.

Dong, X., Li, J., Fu, J. S., Gao, Y., Huang, K., and Zhuang, G.: In-organic aerosols responses to emission changes in Yangtze River Delta, China, Sci. Total Environ., 481, 522–532, 2014.

Edwards, P., Aikin, K. C., Dube, W. P., Fry, J. L., Gilman, J. B., De Gouw, J. A., Graus, M., Hanisco, T. F., Holloway, J. S., and Hubler, G.: Transition from high- to low-NO_x control of night-time oxidation in the southeastern US, Nat. Geosci., 10, 490–495, 2017.

Edwards, P. M., Brown, S. S., Roberts, J. M., Ahmadov, R., Banta, R. M., deGouw, J. A., Dubé, W. P., Field, R. A., Flynn, J. H., Gilman, J. B., Graus, M., Helmig, D., Koss, A., Langford, A. O., Lefer, B. L., Lerner, B. M., Li, R., Li, S.-M., McKeen, S. A., Murphy, S. M., Parrish, D. D., Senff, C. J., Soltis, J., Stutz, J., Sweeney, C., Thompson, C. R., Trainer, M. K., Tsai, C., Veres, P. R., Washenfelder, R. A., Warneke, C., Wild, R. J., Young, C. J., Yuan, B., and Zamora, R.: High winter ozone pollution from carbonyl photolysis in an oil and gas basin, Nature, 514, 351, https://doi.org/10.1038/nature13767, 2014.

Ervens, B., George, C., Williams, J. E., Buxton, G. V., Salmon, G. A., Bydder, M., Wilkinson, F., Dentener, F., Mirabel, P., Wolke, R., and Herrmann, H.: CAPRAM 2.4 (MODAC mechanism): An extended and condensed tropospheric aqueous phase mechanism and its application, J. Geophys. Res.-Atmos., 108, 4426, https://doi.org/10.1029/2002JD002202, 2003.

Fountoukis, C. and Nenes, A.: ISORROPIA II: a computa-tionally efficient thermodynamic equilibrium model for K^+–Ca^{2+}–Mg^{2+}–NH_4^+–Na^+–SO_4^{2-}–NO_3^-–Cl^-–H_2O aerosols, At-mos. Chem. Phys., 7, 4639–4659, https://doi.org/10.5194/acp-7-4639-2007, 2007.

Franchin, A., Fibiger, D. L., Goldberger, L., McDuffie, E. E., Moravek, A., Womack, C. C., Crosman, E. T., Docherty, K. S., Dube, W. P., Hoch, S. W., Lee, B. H., Long, R., Murphy, J. G., Thornton, J. A., Brown, S. S., Baasandorj, M., and Middlebrook, A. M.: Airborne and ground-based observations of ammonium-nitrate-dominated aerosols in a shallow boundary layer during in-tense winter pollution episodes in northern Utah, Atmos. Chem. Phys., 18, 17259–17276, https://doi.org/10.5194/acp-18-17259-2018, 2018.

Fu, X., Wang, T., Gao, J., Wang, P., Liu, Y., Wang, S., Zhao, B., and Xue, L.: Persistent Heavy Winter Nitrate Pollution Driven by Increased Photochemical Oxidants in Northern China, Environ. Sci. Technol., 54, 3881–3889, https://doi.org/10.1021/acs.est.9b07248, 2020.

Gen, M., Zhang, R., Huang, D. D., Li, Y., and Chan, C. K.: Het-erogeneous SO_2 Oxidation in Sulfate Formation by Photoly-sis of Particulate Nitrate, Environ. Sci. Tech. Lett., 6, 86–91, https://doi.org/10.1021/acs.estlett.8b00681, 2019.

Geyer, A. and Stutz, J.: Vertical profiles of NO_3, N_2O_5, O_3, and NO_x in the nocturnal boundary layer: 2. Model studies on the altitude dependence of composition and chemistry, J. Geophys. Res., 109, D12307, https://doi.org/10.1029/2003JD004211, 2004.

Griffith, S. M., Huang, X. H. H., Louie, P. K. K., and Yu, J. Z.: Char-acterizing the thermodynamic and chemical composition factors controlling $PM_{2.5}$ nitrate: Insights gained from two years of on-line measurements in Hong Kong, Atmos. Environ., 122, 864–875, https://doi.org/10.1016/j.atmosenv.2015.02.009, 2015.

Guo, H., Otjes, R., Schlag, P., Kiendler-Scharr, A., Nenes, A., and Weber, R. J.: Effectiveness of ammonia reduction on control

of fine particle nitrate, Atmos. Chem. Phys., 18, 12241–12256, https://doi.org/10.5194/acp-18-12241-2018, 2018.

Hou, X., Chan, C., Dong, G., and Yim, S.: Impacts of transbound-ary air pollution and local emissions on $PM_{2.5}$ pollution in the Pearl River Delta region of China and the public health, and the policy implications, Environ. Res. Lett., 14, 034005, https://doi.org/10.1088/1748-9326/aaf493, 2019.

Hu, W., Hu, M., Hu, W., Jimenez, J. L., Yuan, B., Chen, W., Wang, M., Wu, Y., Chen, C., Wang, Z., Peng, J., Zeng, L., and Shao, M.: Chemical composition, sources, and aging pro-cess of submicron aerosols in Beijing: Contrast between sum-mer and winter, J. Geophys. Res.-Atmos., 121, 1955–1977, https://doi.org/10.1002/2015JD024020, 2016.

Jacob, D. J.: Heterogeneous chemistry and tropospheric ozone, At-mos. Environ., 34, 2131–2159, https://doi.org/10.1016/S1352-2310(99)00462-8, 2000.

Jenkin, M. E., Saunders, S. M., Wagner, V., and Pilling, M. J.: Protocol for the development of the Master Chemical Mecha-nism, MCM v3 (Part B): tropospheric degradation of aromatic volatile organic compounds, Atmos. Chem. Phys., 3, 181–193, https://doi.org/10.5194/acp-3-181-2003, 2003.

Lawal, A. S., Guan, X., Liu, C., Henneman, L. R. F., Vasilakos, P., Bhogineni, V., Weber, R. J., Nenes, A., and Russell, A. G.: Linked Response of Aerosol Acidity and Ammonia to SO_2 and NO_x Emissions Reductions in the United States, Environ. Sci. Technol., 52, 9861–9873, https://doi.org/10.1021/acs.est.8b00711, 2018.

Li, H., Zhang, Q., Zheng, B., Chen, C., Wu, N., Guo, H., Zhang, Y., Zheng, Y., Li, X., and He, K.: Nitrate-driven urban haze pollution during summertime over the North China Plain, At-mos. Chem. Phys., 18, 5293–5306, https://doi.org/10.5194/acp-18-5293-2018, 2018.

Li, L., Lu, C., Chan, P.-W., Zhang, X., Yang, H.-L., Lan, Z.-J., Zhang, W.-H., Liu, Y.-W., Pan, L., and Zhang, L.: Tower observed vertical distribution of $PM_{2.5}$, O_3 and NO_x in the Pearl River Delta, Atmos. Environ., 220, 117083, https://doi.org/10.1016/j.atmosenv.2019.117083, 2020.

Li, S. M., Anlauf, K., and Wiebe, H.: Heterogeneous nighttime production and deposition of particle nitrate at a rural site in North America during summer 1988, J. Geophys. Res.-Atmos., 98, 5139–5157, 1993.

Lin, Y.-C., Zhang, Y.-L., Fan, M.-Y., and Bao, M.: Heteroge-neous formation of particulate nitrate under ammonium-rich regimes during the high-$PM_{2.5}$ events in Nanjing, China, At-mos. Chem. Phys., 20, 3999–4011, https://doi.org/10.5194/acp-20-3999-2020, 2020.

Liu, J., Ren, C., Huang, X., Nie, W., Wang, J., Sun, P., Chi, X., and Ding, A.: Increased Aerosol Extinction Efficiency Hinders Vis-ibility Improvement in Eastern China, Geophys. Res. Lett., 47, e2020GL090167, https://doi.org/10.1029/2020GL090167, 2020.

Liu, J., Liu, Z., Ma, Z., Yang, S., Yao, D., Zhao, S., Hu, B., Tang, G., Sun, J., Cheng, M., Xu, Z., and Wang, Y.: Detailed budget analysis of HONO in Beijing, China: Implication on atmosphere oxidation capacity in polluted megacity, Atmos. Environ., 244, 117957, https://doi.org/10.1016/j.atmosenv.2020.117957, 2021.

Liu, M., Huang, X., Song, Y., Tang, J., Cao, J., Zhang, X., Zhang, Q., Wang, S., Xu, T., Kang, L., Cai, X., Zhang, H., Yang, F., Wang, H., Yu, J. Z., Lau, A. K. H., He, L., Huang, X., Duan, L., Ding, A., Xue, L., Gao, J., Liu, B., and Zhu, T.: Ammonia emis-

sion control in China would mitigate haze pollution and nitrogen deposition, but worsen acid rain, P. Natl. Acad. Sci. USA, 116, 7760, https://doi.org/10.1073/pnas.1814880116, 2019.

Liu, X., Sun, K., Qu, Y., Hu, M., Sun, Y., Zhang, F., and Zhang, Y.: Secondary formation of sulfate and nitrate during a haze episode in megacity Beijing, China, Aerosol Air Qual. Res, 15, 2246–2257, 2015.

Liu, X., Lyu, X., Wang, Y., Jiang, F., and Guo, H.: Intercomparison of O_3 formation and radical chemistry in the past decade at a suburban site in Hong Kong, Atmos. Chem. Phys., 19, 5127–5145, https://doi.org/10.5194/acp-19-5127-2019, 2019.

Lu, K. D., Rohrer, F., Holland, F., Fuchs, H., Bohn, B., Brauers, T., Chang, C. C., Häseler, R., Hu, M., Kita, K., Kondo, Y., Li, X., Lou, S. R., Nehr, S., Shao, M., Zeng, L. M., Wahner, A., Zhang, Y. H., and Hofzumahaus, A.: Observation and modelling of OH and HO_2 concentrations in the Pearl River Delta 2006: a missing OH source in a VOC rich atmosphere, Atmos. Chem. Phys., 12, 1541–1569, https://doi.org/10.5194/acp-12-1541-2012, 2012.

Lu, K., Fuchs, H., Hofzumahaus, A., Tan, Z., Wang, H., Zhang, L., Schmitt, S. H., Rohrer, F., Bohn, B., Broch, S., Dong, H., Gkatzelis, G. I., Hohaus, T., Holland, F., Li, X., Liu, Y., Liu, Y., Ma, X., Novelli, A., Schlag, P., Shao, M., Wu, Y., Wu, Z., Zeng, L., Hu, M., Kiendler-Scharr, A., Wahner, A., and Zhang, Y.: Fast Photochemistry in Wintertime Haze: Consequences for Pollution Mitigation Strategies, Environ. Sci. Technol., 53, 10676–10684, https://doi.org/10.1021/acs.est.9b02422, 2019.

Lu, K. D., Hofzumahaus, A., Holland, F., Bohn, B., Brauers, T., Fuchs, H., Hu, M., Häseler, R., Kita, K., Kondo, Y., Li, X., Lou, S. R., Oebel, A., Shao, M., Zeng, L. M., Wahner, A., Zhu, T., Zhang, Y. H., and Rohrer, F.: Missing OH source in a suburban environment near Beijing: observed and modelled OH and HO_2 concentrations in summer 2006, Atmos. Chem. Phys., 13, 1057–1080, https://doi.org/10.5194/acp-13-1057-2013, 2013.

Lu, X., Chen, N., Wang, Y., Cao, W., Zhu, B., Yao, T., Fung, J. C. H., and Lau, A. K. H.: Radical budget and ozone chemistry during autumn in the atmosphere of an urban site in central China, J. Geophys. Res.-Atmos., 122, 3672–3685, https://doi.org/10.1002/2016JD025676, 2017.

Lyu, X., Wang, N., Guo, H., Xue, L., Jiang, F., Zeren, Y., Cheng, H., Cai, Z., Han, L., and Zhou, Y.: Causes of a continuous summertime O_3 pollution event in Jinan, a central city in the North China Plain, Atmos. Chem. Phys., 19, 3025–3042, https://doi.org/10.5194/acp-19-3025-2019, 2019.

Lyu, X. P., Zeng, L. W., Guo, H., Simpson, I. J., Ling, Z. H., Wang, Y., Murray, F., Louie, P. K. K., Saunders, S. M., Lam, S. H. M., and Blake, D. R.: Evaluation of the effectiveness of air pollution control measures in Hong Kong, Environ. Pollut., 220, 87–94, https://doi.org/10.1016/j.envpol.2016.09.025, 2017.

Mazzuca, G. M., Ren, X., Loughner, C. P., Estes, M., Crawford, J. H., Pickering, K. E., Weinheimer, A. J., and Dickerson, R. R.: Ozone production and its sensitivity to NO_x and VOCs: results from the DISCOVER-AQ field experiment, Houston 2013, Atmos. Chem. Phys., 16, 14463–14474, https://doi.org/10.5194/acp-16-14463-2016, 2016.

McDuffie, E. E., Fibiger, D. L., Dubé, W. P., Lopez-Hilfiker, F., Lee, B. H., Thornton, J. A., Shah, V., Jaeglé, L., Guo, H., Weber, R. J., Michael Reeves, J., Weinheimer, A. J., Schroder, J. C., Campuzano-Jost, P., Jimenez, J. L., Dibb, J. E., Veres, P., Ebben, C., Sparks, T. L., Wooldridge, P. J., Cohen, R.

C., Hornbrook, R. S., Apel, E. C., Campos, T., Hall, S. R., Ullmann, K., and Brown, S. S.: Heterogeneous N_2O_5 Uptake During Winter: Aircraft Measurements During the 2015 WINTER Campaign and Critical Evaluation of Current Parameterizations, J. Geophys. Res.-Atmos., 123, 4345–4372, https://doi.org/10.1002/2018JD028336, 2018a.

McDuffie, E. E., Fibiger, D. L., Dubé, W. P., Lopez Hilfiker, F., Lee, B. H., Jaeglé, L., Guo, H., Weber, R. J., Reeves, J. M., Weinheimer, A. J., Schroder, J. C., Campuzano-Jost, P., Jimenez, J. L., Dibb, J. E., Veres, P., Ebben, C., Sparks, T. L., Wooldridge, P. J., Cohen, R. C., Campos, T., Hall, S. R., Ullmann, K., Roberts, J. M., Thornton, J. A., and Brown, S. S.: $ClNO_2$ Yields From Aircraft Measurements During the 2015 WINTER Campaign and Critical Evaluation of the Current Parameterization, J. Geophys. Res.-Atmos., 123, 12994–913015, https://doi.org/10.1029/2018JD029358, 2018b.

McDuffie, E. E., Womack, C. C., Fibiger, D. L., Dube, W. P., Franchin, A., Middlebrook, A. M., Goldberger, L., Lee, B. H., Thornton, J. A., Moravek, A., Murphy, J. G., Baasandorj, M., and Brown, S. S.: On the contribution of nocturnal heterogeneous reactive nitrogen chemistry to particulate matter formation during wintertime pollution events in Northern Utah, Atmos. Chem. Phys., 19, 9287–9308, https://doi.org/10.5194/acp-19-9287-2019, 2019.

Mozurkewich, M.: The dissociation constant of ammonium nitrate and its dependence on temperature, relative humidity and particle size, Atmos. Environ. A.-Gen., 27, 261–270, https://doi.org/10.1016/0960-1686(93)90356-4, 1993.

Nenes, A., Pandis, S. N., Weber, R. J., and Russell, A.: Aerosol pH and liquid water content determine when particulate matter is sensitive to ammonia and nitrate availability, Atmos. Chem. Phys., 20, 3249–3258, https://doi.org/10.5194/acp-20-3249-2020, 2020.

Novak, G. A. and Bertram, T. H.: Reactive VOC Production from Photochemical and Heterogeneous Reactions Occurring at the Air–Ocean Interface, Accounts Chem. Res., 53, 1014–1023, https://doi.org/10.1021/acs.accounts.0c00095, 2020.

Pathak, R. K., Wu, W. S., and Wang, T.: Summertime $PM_{2.5}$ ionic species in four major cities of China: nitrate formation in an ammonia-deficient atmosphere, Atmos. Chem. Phys., 9, 1711–1722, https://doi.org/10.5194/acp-9-1711-2009, 2009.

Pathak, R. K., Wang, T., and Wu, W. S.: Nighttime enhancement of $PM_{2.5}$ nitrate in ammonia-poor atmospheric conditions in Beijing and Shanghai: Plausible contributions of heterogeneous hydrolysis of N_2O_5 and HNO_3 partitioning, Atmos. Environ., 45, 1183–1191, https://doi.org/10.1016/j.atmosenv.2010.09.003, 2011.

Prabhakar, G., Parworth, C. L., Zhang, X., Kim, H., Young, D. E., Beyersdorf, A. J., Ziemba, L. D., Nowak, J. B., Bertram, T. H., Faloona, I. C., Zhang, Q., and Cappa, C. D.: Observational assessment of the role of nocturnal residual-layer chemistry in determining daytime surface particulate nitrate concentrations, Atmos. Chem. Phys., 17, 14747–14770, https://doi.org/10.5194/acp-17-14747-2017, 2017.

Qin, Y. M., Tan, H. B., Li, Y. J., Schurman, M. I., Li, F., Canonaco, F., Prévôt, A. S. H., and Chan, C. K.: Impacts of traffic emissions on atmospheric particulate nitrate and organics at a downwind site on the periphery of Guangzhou, China, Atmos. Chem.

Phys., 17, 10245–10258, https://doi.org/10.5194/acp-17-10245-2017, 2017.

Riedel, T. P., Wolfe, G. M., Danas, K. T., Gilman, J. B., Kuster, W. C., Bon, D. M., Vlasenko, A., Li, S.-M., Williams, E. J., Lerner, B. M., Veres, P. R., Roberts, J. M., Holloway, J. S., Lefer, B., Brown, S. S., and Thornton, J. A.: An MCM modeling study of nitryl chloride ($ClNO_2$) impacts on oxidation, ozone production and nitrogen oxide partitioning in polluted continental outflow, Atmos. Chem. Phys., 14, 3789–3800, https://doi.org/10.5194/acp-14-3789-2014, 2014.

Romer, P. S., Wooldridge, P. J., Crounse, J. D., Kim, M. J., Wennberg, P. O., Dibb, J. E., Scheuer, E., Blake, D. R., Meinardi, S., Brosius, A. L., Thames, A. B., Miller, D. O., Brune, W. H., Hall, S. R., Ryerson, T. B., and Cohen, R. C.: Constraints on Aerosol Nitrate Photolysis as a Potential Source of HONO and NO_x, Environ. Sci. Technol., 52, 13738–13746, https://doi.org/10.1021/acs.est.8b03861, 2018.

Saunders, S. M., Jenkin, M. E., Derwent, R. G., and Pilling, M. J.: Protocol for the development of the Master Chemical Mechanism, MCM v3 (Part A): tropospheric degradation of non-aromatic volatile organic compounds, Atmos. Chem. Phys., 3, 161–180, https://doi.org/10.5194/acp-3-161-2003, 2003.

Stelson, A. W. and Seinfeld, J. H.: Relative humidity and temperature dependence of the ammonium nitrate dissociation constant, Atmos. Environ., 16, 983–992, https://doi.org/10.1016/0004-6981(82)90184-6, 1982.

Su, T., Li, J., Tian, C., Zong, Z., Chen, D., and Zhang, G.: Source and formation of fine particulate nitrate in South China: Constrained by isotopic modeling and on-line trace gas analysis, Atmos. Environ., 231, 117563, https://doi.org/10.1016/j.atmosenv.2020.117563, 2020.

Tan, Z., Lu, K., Jiang, M., Su, R., Dong, H., Zeng, L., Xie, S., Tan, Q., and Zhang, Y.: Exploring ozone pollution in Chengdu, southwestern China: A case study from radical chemistry to O_3-VOC-NO_x sensitivity, Sci. Total Environ., 636, 775–786, https://doi.org/10.1016/j.scitotenv.2018.04.286, 2018.

Tang, G., Wang, Y., Liu, Y., Wu, S., Huang, X., Yang, Y., Wang, Y., Ma, J., Bao, X., Liu, Z., Ji, D., Li, T., Li, X., and Wang, Y.: Low particulate nitrate in the residual layer in autumn over the North China Plain, Sci. Total Environ., 782, 146845, https://doi.org/10.1016/j.scitotenv.2021.146845, 2021.

Tao, J., Zhang, Z., Tan, H., Zhang, L., Wu, Y., Sun, J., Che, H., Cao, J., Cheng, P., Chen, L., and Zhang, R.: Observational evidence of cloud processes contributing to daytime elevated nitrate in an urban atmosphere, Atmos. Environ., 186, 209–215, https://doi.org/10.1016/j.atmosenv.2018.05.040, 2018.

Tao, Y., Ye, X., Ma, Z., Xie, Y., Wang, R., Chen, J., Yang, X., and Jiang, S.: Insights into different nitrate formation mechanisms from seasonal variations of secondary inorganic aerosols in Shanghai, Atmos. Environ., 145, 1–9, https://doi.org/10.1016/j.atmosenv.2016.09.012, 2016.

von Bobrutzki, K., Braban, C. F., Famulari, D., Jones, S. K., Blackall, T., Smith, T. E. L., Blom, M., Coe, H., Gallagher, M., Ghalaieny, M., McGillen, M. R., Percival, C. J., Whitehead, J. D., Ellis, R., Murphy, J., Mohacsi, A., Pogany, A., Junninen, H., Rantanen, S., Sutton, M. A., and Nemitz, E.: Field inter-comparison of eleven atmospheric ammonia measurement techniques, Atmos. Meas. Tech., 3, 91–112, https://doi.org/10.5194/amt-3-91-2010, 2010.

Wang, C., Yuan, B., Wu, C., Wang, S., Qi, J., Wang, B., Wang, Z., Hu, W., Chen, W., Ye, C., Wang, W., Sun, Y., Wang, C., Huang, S., Song, W., Wang, X., Yang, S., Zhang, S., Xu, W., Ma, N., Zhang, Z., Jiang, B., Su, H., Cheng, Y., Wang, X., and Shao, M.: Measurements of higher alkanes using NO+ chemical ionization in PTR-ToF-MS: important contributions of higher alkanes to secondary organic aerosols in China, Atmos. Chem. Phys., 20, 14123–14138, https://doi.org/10.5194/acp-20-14123-2020, 2020a.

Wang, H., Lu, K., Chen, X., Zhu, Q., Chen, Q., Guo, S., Jiang, M., Li, X., Shang, D., Tan, Z., Wu, Y., Wu, Z., Zou, Q., Zheng, Y., Zeng, L., Zhu, T., Hu, M., and Zhang, Y.: High N_2O_5 Concentrations Observed in Urban Beijing: Implications of a Large Nitrate Formation Pathway, Environ. Sci. Tech. Lett., 4, 416-420, https://doi.org/10.1021/acs.estlett.7b00341, 2017a.

Wang, H., Lu, K., Tan, Z., Sun, K., Li, X., Hu, M., Shao, M., Zeng, L., Zhu, T., and Zhang, Y.: Model simulation of NO_3, N_2O_5 and $ClNO_2$ at a rural site in Beijing during CAREBeijing-2006, Atmos. Res., 196, 97–107, https://doi.org/10.1016/j.atmosres.2017.06.013, 2017b.

Wang, H., Lu, K., Chen, X., Zhu, Q., Wu, Z., Wu, Y., and Sun, K.: Fast particulate nitrate formation via N_2O_5 uptake aloft in winter in Beijing, Atmos. Chem. Phys., 18, 10483–10495, https://doi.org/10.5194/acp-18-10483-2018, 2018a.

Wang, H., Lu, K., Guo, S., Wu, Z., Shang, D., Tan, Z., Wang, Y., Le Breton, M., Lou, S., Tang, M., Wu, Y., Zhu, W., Zheng, J., Zeng, L., Hallquist, M., Hu, M., and Zhang, Y.: Efficient N_2O_5 uptake and NO_3 oxidation in the outflow of urban Beijing, Atmos. Chem. Phys., 18, 9705–9721, https://doi.org/10.5194/acp-18-9705-2018, 2018b.

Wang, N., Guo, H., Jiang, F., Ling, Z. H., and Wang, T.: Simulation of ozone formation at different elevations in mountainous area of Hong Kong using WRF-CMAQ model, Sci. Total Environ., 505, 939–951, https://doi.org/10.1016/j.scitotenv.2014.10.070, 2015.

Wang, N., Lyu, X., Deng, X., Huang, X., Jiang, F., and Ding, A.: Aggravating O_3 pollution due to NO_x emission control in eastern China, Sci. Total Environ., 677, 732–744, https://doi.org/10.1016/j.scitotenv.2019.04.388, 2019.

Wang, Y., Zhang, Y., Hao, J., and Luo, M.: Seasonal and spatial variability of surface ozone over China: contributions from background and domestic pollution, Atmos. Chem. Phys., 11, 3511–3525, https://doi.org/10.5194/acp-11-3511-2011, 2011.

Wang, Z., Yuan, B., Ye, C., Roberts, J., Wisthaler, A., Lin, Y., Li, T., Wu, C., Peng, Y., Wang, C., Wang, S., Yang, S., Wang, B., Qi, J., Wang, C., Song, W., Hu, W., Wang, X., Xu, W., Ma, N., Kuang, Y., Tao, J., Zhang, Z., Su, H., Cheng, Y., Wang, X., and Shao, M.: High Concentrations of Atmospheric Isocyanic Acid (HNCO) Produced from Secondary Sources in China, Environ. Sci. Technol., 54, 11818–11826, https://doi.org/10.1021/acs.est.0c02843, 2020b.

Watson, J. G.: Visibility: Science and Regulation, J. Air Waste Manage., 52, 973–999, 2002.

Wen, L., Chen, J., Yang, L., Wang, X., Caihong, X., Sui, X., Yao, L., Zhu, Y., Zhang, J., Zhu, T., and Wang, W.: Enhanced formation of fine particulate nitrate at a rural site on the North China Plain in summer: The important roles of ammonia and ozone, Atmos. Environ., 101, 294–302, https://doi.org/10.1016/j.atmosenv.2014.11.037, 2015.

Wen, L., Xue, L., Wang, X., Xu, C., Chen, T., Yang, L., Wang, T., Zhang, Q., and Wang, W.: Summertime fine particulate nitrate pollution in the North China Plain: increasing trends, formation mechanisms and implications for control policy, Atmos. Chem. Phys., 18, 11261–11275, https://doi.org/10.5194/acp-18-11261-2018, 2018.

Wolfe, G. M., Marvin, M. R., Roberts, S. J., Travis, K. R., and Liao, J.: The Framework for 0-D Atmospheric Modeling (F0AM) v3.1, Geosci. Model Dev., 9, 3309–3319, https://doi.org/10.5194/gmd-9-3309-2016, 2016.

Womack, C. C., McDuffie, E. E., Edwards, P. M., Bares, R., de Gouw, J. A., Docherty, K. S., Dube, W. P., Fibiger, D. L., Franchin, A., Gilman, J. B., Goldberger, L., Lee, B. H., Lin, J. C., Long, R., Middlebrook, A. M., Millet, D. B., Moravek, A., Murphy, J. G., Quinn, P. K., Riedel, T. P., Roberts, J. M., Thornton, J. A., Valin, L. C., Veres, P. R., Whitehill, A. R., Wild, R. J., Warneke, C., Yuan, B., Baasandorj, M., and Brown, S. S.: An odd oxygen framework for wintertime ammonium nitrate aerosol pollution in urban areas: NO$_x$ and VOC control as mitigation strategies, Geophys. Res. Lett., 46, 4971–4979, https://doi.org/10.1029/2019gl082028, 2019.

Wu, C., Wang, C., Wang, S., Wang, W., Yuan, B., Qi, J., Wang, B., Wang, H., Wang, C., Song, W., Wang, X., Hu, W., Lou, S., Ye, C., Peng, Y., Wang, Z., Huangfu, Y., Xie, Y., Zhu, M., Zheng, J., Wang, X., Jiang, B., Zhang, Z., and Shao, M.: Measurement report: Important contributions of oxygenated compounds to emissions and chemistry of volatile organic compounds in urban air, Atmos. Chem. Phys., 20, 14769–14785, https://doi.org/10.5194/acp-20-14769-2020, 2020.

Xu, L. and Penner, J. E.: Global simulations of nitrate and ammonium aerosols and their radiative effects, Atmos. Chem. Phys., 12, 9479–9504, https://doi.org/10.5194/acp-12-9479-2012, 2012.

Xue, J., Yuan, Z., Lau, A. K. H., and Yu, J. Z.: Insights into factors affecting nitrate in PM$_{2.5}$ in a polluted high NO$_x$ environment through hourly observations and size distribution measurements, J. Geophys. Res.-Atmos., 119, 4888–4902, https://doi.org/10.1002/2013JD021108, 2014a.

Xue, L. K., Wang, T., Gao, J., Ding, A. J., Zhou, X. H., Blake, D. R., Wang, X. F., Saunders, S. M., Fan, S. J., Zuo, H. C., Zhang, Q. Z., and Wang, W. X.: Ground-level ozone in four Chinese cities: precursors, regional transport and heterogeneous processes, Atmos. Chem. Phys., 14, 13175–13188, https://doi.org/10.5194/acp-14-13175-2014, 2014b.

Yang, Q., Su, H., Li, X., Cheng, Y., Lu, K., Cheng, P., Gu, J., Guo, S., Hu, M., and Zeng, L.: Daytime HONO formation in the suburban area of the megacity Beijing, China, Science China Chemistry, 57, 1032–1042, 2014.

Yang, T., Sun, Y., Zhang, W., Wang, Z., Liu, X., Fu, P., and Wang, X.: Evolutionary processes and sources of high-nitrate haze episodes over Beijing, Spring, J. Environ. Sci., 54, 142–151, https://doi.org/10.1016/j.jes.2016.04.024, 2017.

Ye, C., Gao, H., Zhang, N., and Zhou, X.: Photolysis of Nitric Acid and Nitrate on Natural and Artificial Surfaces, Environ. Sci. Technol., 50, 3530–3536, https://doi.org/10.1021/acs.est.5b05032, 2016.

Ye, C., Zhang, N., Gao, H., and Zhou, X.: Photolysis of Particulate Nitrate as a Source of HONO and NO$_x$, Environ. Sci. Technol., 51, 6849–6856, https://doi.org/10.1021/acs.est.7b00387, 2017.

Ye, C., Yuan, B., Lin, Y., Wang, Z., Hu, W., Li, T., Chen, W., Wu, C., Wang, C., Huang, S., Qi, J., Wang, B., Wang, C., Song, W., Wang, X., Zheng, E., Krechmer, J. E., Ye, P., Zhang, Z., Wang, X., Worsnop, D. R., and Shao, M.: Chemical characterization of oxygenated organic compounds in the gas phase and particle phase using iodide CIMS with FIGAERO in urban air, Atmos. Chem. Phys., 21, 8455–8478, https://doi.org/10.5194/acp-21-8455-2021, 2021.

Yu, C., Wang, Z., Xia, M., Fu, X., Wang, W., Tham, Y. J., Chen, T., Zheng, P., Li, H., Shan, Y., Wang, X., Xue, L., Zhou, Y., Yue, D., Ou, Y., Gao, J., Lu, K., Brown, S. S., Zhang, Y., and Wang, T.: Heterogeneous N$_2$O$_5$ reactions on atmospheric aerosols at four Chinese sites: improving model representation of uptake parameters, Atmos. Chem. Phys., 20, 4367–4378, https://doi.org/10.5194/acp-20-4367-2020, 2020.

Yu, Y., Cheng, P., Li, H., Yang, W., Han, B., Song, W., Hu, W., Wang, X., Yuan, B., Shao, M., Huang, Z., Li, Z., Zheng, J., Wang, H., and Yu, X.: Budget of nitrous acid (HONO) and its impacts on atmospheric oxidation capacity at an urban site in the fall season of Guangzhou, China, Atmos. Chem. Phys. Discuss. [preprint], https://doi.org/10.5194/acp-2021-178, in review, 2021.

Yuan, B., Chen, W., Shao, M., Wang, M., Lu, S., Wang, B., Liu, Y., Chang, C., and Wang, B.: Measurements of ambient hydrocarbons and carbonyls in the Pearl River Delta (PRD), China, Atmos. Res., 116, 93–104, 2012.

Yuan, B., Liggio, J., Wentzell, J., Li, S.-M., Stark, H., Roberts, J. M., Gilman, J., Lerner, B., Warneke, C., Li, R., Leithead, A., Osthoff, H. D., Wild, R., Brown, S. S., and de Gouw, J. A.: Secondary formation of nitrated phenols: insights from observations during the Uintah Basin Winter Ozone Study (UBWOS) 2014, Atmos. Chem. Phys., 16, 2139–2153, https://doi.org/10.5194/acp-16-2139-2016, 2016.

Yun, H., Wang, T., Wang, W., Tham, Y. J., Li, Q., Wang, Z., and Poon, S. C. N.: Nighttime NO$_x$ loss and ClNO$_2$ formation in the residual layer of a polluted region: Insights from field measurements and an iterative box model, Sci. Total Environ., 622–623, 727–734, https://doi.org/10.1016/j.scitotenv.2017.11.352, 2018a.

Yun, H., Wang, W., Wang, T., Xia, M., Yu, C., Wang, Z., Poon, S. C. N., Yue, D., and Zhou, Y.: Nitrate formation from heterogeneous uptake of dinitrogen pentoxide during a severe winter haze in southern China, Atmos. Chem. Phys., 18, 17515–17527, https://doi.org/10.5194/acp-18-17515-2018, 2018b.

Zhai, S., Jacob, D. J., Wang, X., Liu, Z., Wen, T., Shah, V., Li, K., Moch, J. M., Bates, K. H., Song, S., Shen, L., Zhang, Y., Luo, G., Yu, F., Sun, Y., Wang, L., Qi, M., Tao, J., Gui, K., Xu, H., Zhang, Q., Zhao, T., Wang, Y., Lee, H. C., Choi, H., and Liao, H.: Control of particulate nitrate air pollution in China, Nat. Geosci., 14, 389–395, https://doi.org/10.1038/s41561-021-00726-z, 2021.

Zhang, H., An, Q., Zhao, S., Xie, B., and Liu, Q.: Advances in the research of optical properties and radiative forcing of nitrate aerosols, Acta Meteorologica Sinica, 75, 539–551, 2017.

Zhang, R., Gen, M., Huang, D., Li, Y., and Chan, C. K.: Enhanced Sulfate Production by Nitrate Photolysis in the Presence of Halide Ions in Atmospheric Particles, Environ. Sci. Technol., 54, 3831–3839, https://doi.org/10.1021/acs.est.9b06445, 2020.

Zhou, S., Wu, L., Guo, J., Chen, W., Wang, X., Zhao, J., Cheng, Y., Huang, Z., Zhang, J., Sun, Y., Fu, P., Jia, S., Tao, J., Chen, Y., and Kuang, J.: Measurement report: Vertical distribution of atmospheric particulate matter within the urban boundary layer in southern China – size-segregated chemical composition and secondary formation through cloud processing and heterogeneous reactions, Atmos. Chem. Phys., 20, 6435–6453, https://doi.org/10.5194/acp-20-6435-2020, 2020.